PL-TR-91-2050

DEVELOPMENT OF A NUMERICAL SCHEME TO PREDICT GEOMAGNETIC STORMS AFTER INTENSE SOLAR EVENTS AND GEOMAGNETIC ACTIVITY 27 DAYS IN ADVANCE

S-I. Akasofu
Li-Her Lee

University of Alaska
Geophysical Institute
Fairbanks, Alaska 99775-0800

February 1991

Final Report
6 August 1986-16 November 1990

PHILLIPS LABORATORY
AIR FORCE SYSTEMS COMMAND
HANSCOM AIR FORCE BASE, MASSACHUSETTS 01731-5000

"This technical report has been reviewed and is approved for publication"

JURGEN BUCHAU
Contract Manager

WILLIAM K. VICKERY
Branch Chief

FOR THE COMMANDER

ROBERT A. SKRIVANEK
Division Director

This report has been reviewed by the ESD Public Affairs Office (PA) and is releasable to the National Technical Information Service (NTIS).

Qualified requestors may obtain additional copies from the Defense Technical Information Center. all others should apply to the National Technical Information Service.

If your address has changed, or if you wish to be removed from the mailing list, or if the addressee is no longer employed by your organization, please notify GL/IMA, Hanscom AFB, MA 01731. This will assist us in maintaining a current mailing list.

Do not return copies of this report unless contractual obligations or notices on a specific document requires that it be returned.

REPORT DOCUMENTATION PAGE

Form Approved
OMB No. 0704-0188

1. AGENCY USE ONLY (Leave blank)	2. REPORT DATE	3. REPORT TYPE AND DATES COVERED
	February 1991	Final Report 8/6/86 - 11/16/90

4. TITLE AND SUBTITLE
Development of a Numerical Scheme to Predict Geomagnetic Storms After Intense Solar Events and Geomagnetic Activity 27 Days in Advance

5. FUNDING NUMBERS
PE 62101F
PR 4643 TA 08 WU AL

Contract F19628-86-K-0030

6. AUTHOR(S)
S-I. Akasofu
Li-Her Lee

7. PERFORMING ORGANIZATION NAME(S) AND ADDRESS(ES)
University of Alaska
Geophysical Institute
Fairbanks, Alaska 99775-0800

8. PERFORMING ORGANIZATION REPORT NUMBER

9. SPONSORING/MONITORING AGENCY NAME(S) AND ADDRESS(ES)
Phillips Laboratory
Hanscom AFB, MA 01731-5000

Contract Manager: Jurgen Buchau/LIS

10. SPONSORING/MONITORING AGENCY REPORT NUMBER
PL-TR-91-2050

11. SUPPLEMENTARY NOTES

12a. DISTRIBUTION/AVAILABILITY STATEMENT
Approved for public release; distribution unlimited

12b. DISTRIBUTION CODE

13. ABSTRACT (Maximum 200 words)

The modern geomagnetic storm prediction scheme should be based on a numerical simulation method, rather than on a statistical result. Furthermore, the scheme should be able to predict the geomagnetic storm indices, such as the Dst and AE indices, as a function of time.

By recognizing that geomagnetic storms are powered by the solar wind-magnetosphere generator and that its power is given in terms of the solar wind speed, the interplanetary magnetic field (IMF) magnitude and polar angle, we have made a major advance in predicting both flare-induced storms and recurrent storms.

Furthermore, it is demonstrated that the prediction scheme can be calibrated using the interplanetary scintilation (IPS) observation, when the solar disturbance advances about half-way to the earth.

It is shown, however, that we are still far from a reliable prediction scheme. The prediction of the IMF polar angle requires future advance in understanding characteristics of magnetic clouds.

14. SUBJECT TERMS	15. NUMBER OF PAGES
Modern prediction scheme for magnetic storms	62
	16. PRICE CODE

17. SECURITY CLASSIFICATION OF REPORT	18. SECURITY CLASSIFICATION OF THIS PAGE	19. SECURITY CLASSIFICATION OF ABSTRACT	20. LIMITATION OF ABSTRACT
Unclassified	Unclassified	Unclassified	SAR

TABLE OF CONTENTS

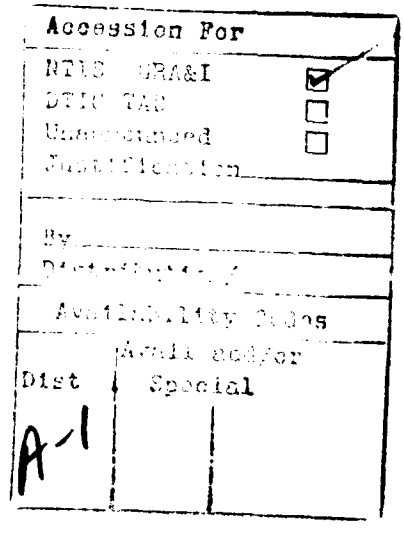

Figure Captions

Figure 1. Geomagnetic and ionospheric storms are caused by two types of solar phenomena. The first one is transient activities, such as solar flares, prominence disappearances, coronal mass ejections, while the second one is a high speed stream from a coronal hole which is the least active region of the sun. Thus, the storm prediction scheme must take both phenomena into account.

Figure 2. There is a considerable spread in the transit time (Ts) of solar disturbances associated with solar flares to reach the earth. The histogram shows that geomagnetic storms can occur about 20 hours after a flare, but can be as late as 70 hours. Therefore, although the mean value of the transit time is 43 hours, such a statistical study is little use for predicting the onset time of a geomagnetic storm after a specific flare.

Figure 3. The modern geomagnetic storm prediction scheme must depend on the latest progress in solar-terrestrial physics, not on statistical results shown in Figure 2. It is based on the fact that a geomagnetic storm results from increased electric currents around the earth, which are, in turn, caused by an increased power of the solar wind-magnetosphere generator.

Figure 4. The modern geomagnetic storm prediction scheme consists of three steps. After parameterizing and quantifying a solar flare, three vital quantities (V, B, θ) are computed at the earth's location in step 1. In step 2, the three values are used to compute the power of the solar wind-magnetosphere generator as a function of time Since the power is related to, empirically or theoretically, to the geomagnetic storm

indices (AE, Pst, Kp), it is possible to predict the the indices as a function of time in step 3.

Figure 5. It is important to be able to calibrate the storm prediction scheme when the responsible solar disturbance reaches about half way to the earth. By monitoring celestrial radio sources (A, B,...F) over the sky, it is now possible to infer the geometry of the advancing solar disturbance, since the solar disturbance (the plasma cloud) causes intense scintillation of radio sources. Details of the scheme is shown in Figure 6.

Figure 6. Based on the six flare parameters of a specific flare, the modern storm prediction scheme can determine the geometry of the advancing solar disturbance. The prediction scheme can then produce the predicted sky map of interplanetary scintillation (IPS) at a given time, say 24 hours after a specific flare. When the observed IPS sky map becomes available, both sky maps can be compared. (In this particular example, the IPS was expected to occur in the western sky, but the observed high (H) scintillation occurred in the eastern sky). By this calibration method, it was found that the responsible flare was misidentified in the first computation; during an active period of sun, many flares take place within a few hours over the solar disk. The correct identification of the responsible flare was confirmed by finding that another flare can reproduce the observed IPS sky map. Based on the new six parameter for that flare, the prediction scheme is carried out to demonstrate that the observed variations of the solar wind speed is very close to the predicted one.

Figure 7A. Comparison of the observed solar wind speed by an earth-bound satellite and the predicted one for the September 25 - October 1, 1978 storm event. In spite of

a very complicated series of events on the sun, the three shock structures are well reproduced by the prediction scheme (see also Figure 6).

Figure 7B. The predicted geometry of the advancing interplanetary disturbance for the storm event illustrated in Figures 6 and 7A. S: Sun, E. Earth.

Figure 7C. The predicted IPS sky map of the advancing interplanetary disturbance for the storm event illustrated in Figures 6, 7A and 7B. Note that the second IPS, caused by a new flare, began on September 25, 1978.

Figure 7D. The observed IPS sky map of the advancing interplanetary disturbance for the storm event illustrated in Figures 6, 7A, 7B and 7C. The high scintillation area is indicated by H. This observation was made by the Cambridge IPS group.

Figure 8A. In the modern storm prediction scheme, the geomagnetic storm indices (AE, Dst, Kp) are estimated empirically on the basis of the computed power of the solar wind-magnetosphere generator (Figure 4). This is because there is so far no reliable theoretical formulation to relate the power to the indices. However, here we attempt to set up an equivalent electrical circuit for the magnetosphere. Thus, by providing the predicted power as a function of time, it will be possible to determine the geomagnetic indices.

Figure 8B. For a given voltage variation (Φ_{CT} (t)), the equivalent circuit can predict variations of the resistance R_T in the magnetotail, the polar cap potential drop (Φ_{ps}) and the energy (W_B) released in the polar ionosphere. From these predicted values, it is possible to infer the geomagnetic indices (see Figure 9).

Figure 9. The equivalent circuit in Figure 8A can predict the potential drop (Φ_{ps}) across the polar cap. There are two important empirical relationships between Φ_{ps} and the AE index, obtained by satellite observations (Weimer, et al.) and ground-based observations (Ahn, et al.). Using this established relationship, it is possible to infer the AE index as a function of time from Φ_{ps}.

Figure 10. We can advance the present geomagnetic storm prediction scheme to include the prediction of ionospheric storms. Once the power of the solar wind-magnetosphere generator is predicted in step 2 (Figure 4), it is possible to predict the potential drop Φ_{pc} across the polar cap, as illustrated in Figures 8A, 8B and 9. Our prediction scheme can also predict the size of the auroral oval. Thus, for a given date and time, the ionosphere storm code can predict the flow of ionospheric plasma across the polar region and the electron density profile at a desired time. Radio ray paths can be computed on the basis of the predicted electron density profile. In this case, a high Φ_{pc} caused an intense flow of ionospheric plasma from the sunlit hemisphere to the dark hemisphere across the polar cap.

Figure 11. Example of the computed electron density profile at an altitude of 300 km. There is a high density in the dayside ionosphere (caused by the solar radiation) and also along the auroral oval (caused by auroral particle precipitation). The dayside plasma flows into the polar cap by the dawn-dusk potential drop (Φ_{pc}) can be seen.

Figure 12A. Simulation result demonstrating how a particular type of disturbance caused at a confined location in a magnetic flux tube propagates. Such a disturbance may be identified as a "magnetic cloud."

Figure 12B. Our prediction scheme has been improved to the point to be able to predict the solar wind speed V and the interplanetary magnetic field (IMF) magnitude B for simple events. The simplest event is illustrated in a) in which the advancing shock wave(s) compresses the existing interplanetary magnetic field in the vicinity of the earth. If the IMF field is directed southward and has a magnitude of 5 nT, the arrival of the shock wave can compress the field, causing a large (~ 15 nT) southward pointing field. Such a high southward field can certainly cause an intense geomagnetic storm. However, the advancing disturbances are often much more complicated. In an exactly opoposite case, an enhanced northward directed field will reduce geomagnetic activity. A number of possibilities are shown here.

Figure 13. During 1974, there were two large coronal halos, from which two high speed streams emanated. During a single solar rotation (27 days), two peaks of the solar wind speed were seen (top). The next two rows shown, the IMF magnitude and the two angles of the IMF (the latitude angle theta and the azimutnal angle phi). On the basis of these observed quantity, the power (ε) of the solar wind-magnetosphere generator is computed. The last two rows show the AE and Dst index, respectivity. There is a fairly good similarity between ε and AE, suggesting that ε can predict the envelope of the AE index.

Figure 14A. The prediction of a high speed stream depends critically on the magnetic field distribution on the so-called "source surface," a spherical surface of radius of 2.5 solar radii. In the right column, sunspot number between 1976 and 1986 is shown. In the middle column, shows how the magnetic neutral line (or the magnetic equator) on the source surface changed during the sunspot cycle. The left column shows the polarity of the magnetic field and the magnetic equator in solar longitude-latitude map (the magnetic field is directed inward in the hatched area).

Figure 14B. In order to predict the geometry of the magnetic neutral line, a simple method is developed to represent the magnetic neutral line. The method uses a central, axially aligned dipole and two (or at most four) dipoles on the photosphere. The observed and reproduced magnetic neutral lines are compared for Carrington rotation 1666.

Figure 15. Once the magnetic neutral line is reasonably reproduced, the prediction of the magnetic neutral line is reduced to the prediction of changes of the two photospheric dipoles in Figure 14B. The figure shows the observed and reproduced magnetic neutral lines for Carrington rotations 1661-1664. In these cases, four photospheric dipoles are used.

Figure 16. In this figure, we follow the location (latitude, longitude), the azimuth angle and magnitude of the photospheric dipole no. 3 in Figure 15. One can see that the changes of the dipole were not erratic. Thus, it was possible to extrapolate changes of the dipole quantities and thus predict changes of the magnetic neutral time during the successive Carrington rotations.

Development of a Numerical Scheme to Predict Geomagnetic Storms After Intense Solar Events and Geomagnetic Activity 27 Days in Advance

S.-I. Akasofu

Geophysical Institute
University of Alaska
Fairbanks AK 99775-0800

SUMMARY

The contract has two major objectives. The first objective is to establish the computer scheme which can predict the occurrence and development of a major geomagnetic storm after an intense solar flare. Since the intensity of geomagnetic storm is given in terms of the geomagnetic indices such as AE, Kp and Dst, a quantitative storm prediction must be able to provide the geomagnetic indices as a function of time for a given solar flare.

The prediction scheme consists of three steps. The first step is an attempt to compute the solar wind speed (V), the interplanetary magnetic field magnitude (B) and the polar angle (θ). The second step computes the power (P) generated by the solar wind-magnetosphere interaction. In the third step the empirical relationship between P and the geomagnetic indices is used to compute the geomagnetic indices as a function of time. At the present time, it is not possible to predict the polar angle of θ of the interplanetary magnetic field. This reduces our scheme to predict the maximum possible power P_m.

- We have completed the solar wind code which predicts the solar wind speed V and the interplanetary magnetic field magnitude B at the front of the magnetosphere even for a complicated situation in which many flares occur in a relatively short period. The two quantities allow us to compute the maximum possible power P_m of the solar wind magnetosphere generator.

- In the prediction scheme, it is important to be able to compare the observed and computed geometry of the shock wave at a midpoint between the sun and the

earth. We have found that the interplanetary scintillation (IPS) can serve for such a purpose. Thus, we have successfully incorporated results from the interplanetary scintillation (IPS) in the prediction scheme. In the code, we can calibrate the initial conditions of a solar flare using the IPS observations.

- Since we can compute $P_m(t)$ as a function of time and since there are empirical relations between P(t) and AE/Kp/Dst, it is possible to predict the maximum AE/Kp/Dst as a function of time.
- Since there is an empirical relationship between P and the cross-polar cap potential Φ_{pc}, it is also possible to infer time variations of the maximum value of Φ_{pc} for a given time variation of P_m.
- We have also developed an equivalent circuit for the magnetosphere. For a given input function P(t) or $P_m(t)$, it is possible to predict AE/Kp/Dst (or the maximum of AE/KP/Dst) as a function of time.
- We have also developed a code to predict the distribution of the F-layer electron density. The F-layer electron density in the polar cap depends crucially on the potential drop Φ_{pc} across the polar cap.

The second objective of this project is to advance the prediction of 27-day recurrent storms.

- We have found that this project is reduced to predict both the solar wind speed and the IMF magnitude 27 days in advance and that this task is further reduced to predict the geometry of the neutral line on the solar source surface (a spherical surface of 2.5 solar radii).
- We have devised a multi-dipole method to reproduce the neutral line.
- Thus, the prediction is finally reduced to predict the growth and decay of the dipoles in low latitude of the photosphere. We have made much progress in understanding the nature of these dipoles.

In summary, altogether we have developed a computer code to execute what is described in the above, our present prediction scheme may be considered to be a 'skeleton structure' for the future scheme. We believe that most of the elements in the prediction scheme are assembled and are properly connected. The method requires much improvement in the future, which depends on the progress, both observational and theoretical, in the field of solar-terrestrial physics. These are summarized in the last section "Concluding Remarks."

1. INTRODUCTION

1.1 General Review

Solar-terrestrial physics has been advanced considerably during the last two decades. The progress has been prominent in almost every discipline, namely studies of solar flares, interplanetary disturbances and magnetospheric disturbances. A transient phenomenon called "coronal mass ejection (CME)" has been discovered (cf. Gosling, et al., 1974; Hildner, et al., 1975, 1976; Sheeley, et al., 1980; Wagner, 1984) and its association with soft x-ray events and other phenomena have been investigated (Sheeley et al., 1983, 1984; Kahler et al., 1984a, b; Burlaga et al., 1982). The source region of high speed solar wind streams, namely the "coronal holes," have also been identified (cf. Zirker, 1977). A study of interplanetary disturbances has been greatly advanced by the availability of in situ observations of the solar wind and the interplanetary magnetic field (IMF) by deep space probes and earth-bound satellites. The interaction between the 'quiet time' solar wind and a high speed solar wind stream, namely the stream-stream interaction, has been studied extensively, both observationally and theoretically (cf. Dryer and Steinolfson, 1976; D'Uston, et al., 1981).

In addition to such progress in each discipline of solar-terrestrial physics, there have been considerable efforts in finding one-to-one relationships between solar activity and interplanetary disturbances and also between interplanetary disturbances and magnetospheric substorms and storms. An extensive study of the relationship between the large-scale magnetic field in the photospheric level and the interplanetary magnetic field in the photospheric level and the interplanetary magnetic field has been made (cf. Wilcox et al., 1980; Hoeksema et al., 1982, 1983). The relationship between solar activity (such as flares and CMEs) and shock waves in interplanetary space has been investigated (Chao and Lepping, 1974; Joselyn and Bryson, 1980; Sheeley et al., 1985). The so-called

"Sudden Disappearing Filaments (SDFs)" have been added as a new possible source of interplanetary magnetospheric disturbances (Schwenn et al., 1983; Joselyn and McIntosh, 1981; Wright and McNamara, 1983; Sanahuja et al., 1983). In solar wind-magnetosphere interaction studies, some of the key physical quantities in the energy transfer processes have been identified. Among these, the north-south component of the IMF is found to play a crucial role in the energy transfer (cf. Arnoldy, 1981; Tsurutani and Meng, 1972; Russell and McPherron, 1973; Meng et al., 1973; Clauer et al., 1981; Akasofu, 1981; Baker et al., 1981; Meloni et al., 1982).

In spite of such progresses in each discipline and in some interdisciplinary areas, our understanding of some of the most crucial aspects of solar-terrestrial physics has not been very much improved. One of such examples is the so-called "driver-gas" which is supposed to be ejected during a solar event and to cause an interplanetary shock wave which causes, in turn, a geomagnetic storm. However, the identification of the "driver-gas" in interplanetary space has not been very conclusive. First of all, only a few plasma ejectas identified in the Hα photographs have been observed to leave the field of view of the camera; some of them simply rain back down to the chromosphere. Tracing of type IV radio bursts which are supposed to be generated by energetic electrons in the 'ejecta' have been limited to about several solar radii. Except for a fairly high correlation, the physical relationship between a CME and a shock wave has not been established yet. Is a CME an early stage of the shock wave, a driven gas or neither of them?

There has also been no agreed common signature of the driver gas from spacecraft measurements. Some workers consider that a high ratio of He/H (or a high concentration of helium) after the passage of the shock waves is an important signature of the "driver gas" (Hirshberg et al., 1970, 1972a, b; Gosling et

al., 1980; Borrini et al., 1982a, b; Zwickl et al., 1983). Others consider a prominent decrease of the proton temperature (Gosling et al., 1973; Zwickl et al., 1983), or a very steady, large magnitude of the interplanetary magnetic field (Smith, 1983) as the most important signature. The so-called "magnetic cloud" proposed by Klein and Burlaga (1982) may also be added as another proposed signature. Bi-directional streaming of solar wind electrons has also been considered as an evidence for a closed field structure within the drive gas (Bame et al., 1981). For a recent review on the plasma properties of the solar wind, see Neugebauer (1983).

A number of MHD simulation studies have also been conducted to predict how the density, temperature and velocity of the disturbed solar wind and IMF vary behind the interplanetary shock waves. The common practice in this particular simulation study is to allow the duration of heat input during a flare to be a variable. An impulsive heat input of duration of 30 min - 1.5 hours into the solar atmosphere simulates the generation of a blast wave, while a constant heat input lasting for at least 40 hours simulates a continuous 'piston-like' process with a shock front (cf. Hundhausen and Gentry, 1969a, b; Dryer, 1970). The simulation studies of the blast waves indicate that it is followed by a large depression of the density and of the IMF magnitude (cf. Wu et al., 1976; D'Uston et al., 1981; Wu et al., 1983; Dryer et al., 1984).

However, such a prominent depression of <u>both</u> the proton density and the IMF magnitude after the passage of the shock waves is not a common occurrence, although the proton density can drop after the passage of several major shocks (Sheeley et al., 1985). For this and other reasons, Borrini et al., (1982b) concluded that there is little evidence that the blast waves actually exist in interplanetary space and that the occurrence of mass ejection events (Hildner et al., 1976) is more than sufficient to account for all shocks observed at 1 AU. Recently, Smart and

Shea (1985) suggested that most of the shock waves are initially driven to a distance of 0.1 AU and then propagate as a blast wave.

Recently, Zwickl et al. (1983) showed that of 54 shocks observed from August 1978 to February 1980, 9 events were followed by a clearly identifiable decrease of the temperature and an increase of the He/H ratio, although the source activity for those chosen 9 events were not identified. Zwickl et al. (1983) also added an increase of the IMF magnitude as a signature of the driver gas. Borrini et al. (1982b) inferred that a high ratio of He/H arises from flares in the vicinity of the central meridian, although their paper does not show any supporting evidence for such an inference.

Geomagnetic/ionospheric storms can be classified into two types, depending on their origin in the solar atmosphere (Fig. 1). The first type is associated with intense eruptions in the solar atmosphere, which are generally called solar flares. It is known, however, that not all flares cause geomagnetic/ionospheric storms. Recent studies have revealed that solar flares followed by soft x-ray emissions of a long duration (of several hours) cause geomagnetic/ionospheric storms (Sheeley et al., 1983, 1984). It is expected that such a flare ejects a gas cloud into interplanetary space. As the driver gas advances into interplanetary space, it generates an interplanetary shock wave. A geomagnetic/ionospheric storm begins when the shock wave and the driver gas collide with the earth's magnetic field. The development of a geomagnetic storm depends on several physical parameters of the driver gas and its relative path with respect to the earth. As we reviewed earlier, our knowledge on the driver gas is still too poor to be used in predicting the development of a geomagnetic storm.

The second type of geomagnetic/ionospheric storms is associated with an intense solar flare wind flow from very quiet regions of the solar corona. Such

regions look very dark when the corona is observed by a soft x-ray camera. It is for this reason that these regions are called 'coronal holes.' It is not known at all why the most quiet region of the solar corona can produce the most intense solar wind. Hakameda (1987) and Wang and Sheeley (1990) showed that the highest speed wind may be related to very limited regions on the photosphere. The life time of coronal holes varies considerably, from less than one month to more than 12 months. A long lasting coronal hole causes geomagnetic storms with an interval of approximately 27 days, as the sun rotates once in 25 days and the earth revolves around the sun in the same direction.

1.2 Needs for a New Prediction Scheme

In the past, most prediction effort of geomagnetic/ionospheric storms had been based on statistical results. For example, the prediction of the onset time of a geomagnetic storm is made on the basis of a statistical result that geomagnetic storms begin most frequently about 43 hours after a responsible flare. Figure 2 shows the histogram which shows the time interval between flare onset and storm onset. Although such a histogram is useful, the spread is too large to be useful in predicting the onset time of a geomagnetic storm after a specific solar event.

Like the modern weather forecasting, the modern prediction scheme should be based on numerical methods for individual events and is based on the following facts (Fig. 3):

(1) The interaction between the solar wind and the earth's magnetic field constitutes a generator.

(2) The power of the generator depends on the solar wind V, the magnitude B and the polar angle θ of the interplanetary magnetic field (Perreault and Akasofu, 1978; Akasofu, 1981).

GEOMAGNETIC AND IONOSPHERIC STORMS

First Type -- associated with Solar Flares

Second Type -- associated with Coronal Holes

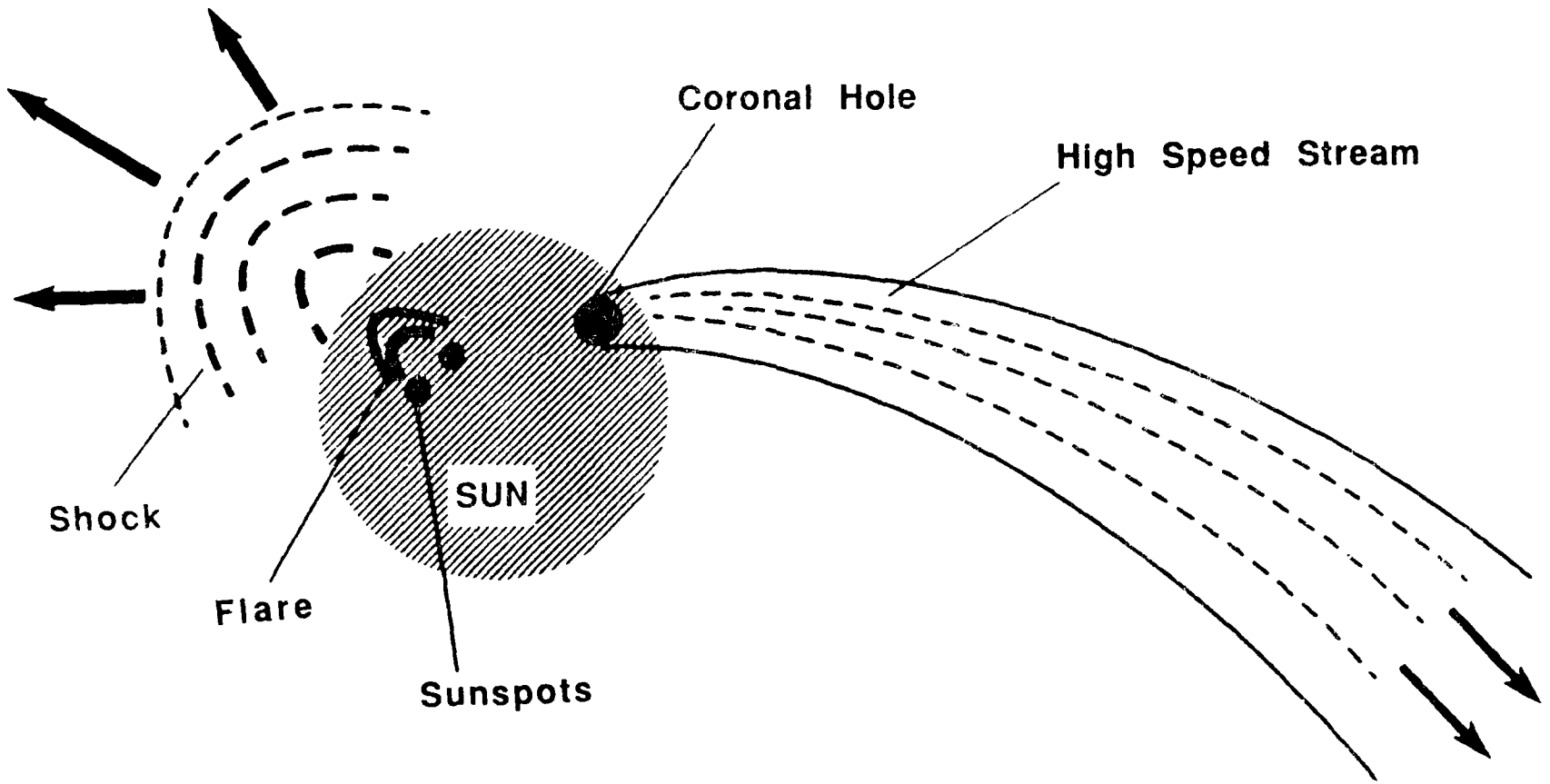

FIGURE 1

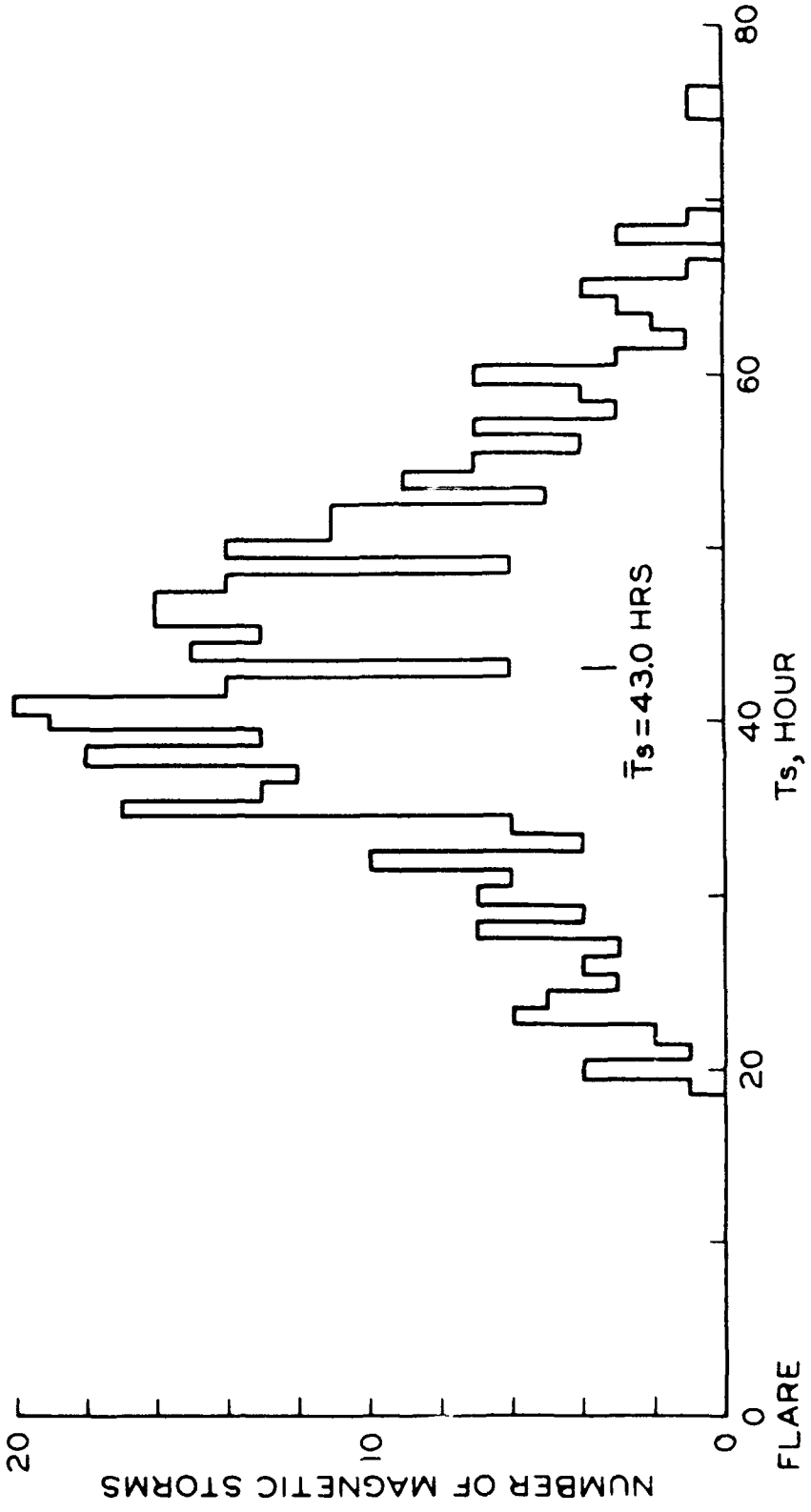
NUMBER OF MAGNETIC STORMS
20
10
0
0
FLARE
20
40
60
80
Ts, HOUR
$\bar{T}s = 43.0$ HRS

FIGURE 2

MODERN GEOMAGNETIC-IONOSPHERIC STORM PREDICTION SCHEME

Based on:

1. **The interaction between the solar wind and the magnetosphere (Earth's magnetic field) constitutes a generator.**

2. **The gusty solar wind increases the power of the generator.**

3. **An increased power causes geomagnetic-ionospheric storms.**

4. **The power is determined by:**
   Power (Mega Watts) = 20V (Km/sec) B^2 (nT) $\sin^4(\theta/2)$.
   - **V = Solar wind speed**
   - **B = Solar wind magnetic field magnitude**
   - **θ = Solar wind magnetic field polar angle**

5. **The modern geomagnetic-ionospheric storm prediction scheme is boiled down to predicting V, B, θ, for a given solar event.**

Figure 3

$$P\ (\text{Mwatts}) = 20\ V\ (\text{km/sec})\ B^2(\text{nT})\ sin^4\ (\theta/2)$$

(3) Thus, having a higher speed V and greater magnitude B of the interplanetary magnetic field, a 'gusty' solar wind (the shock wave/driver gas or of the solar wind flow from the coronal hole) tends to increase the power of the solar wing-magnetosphere generator.

(4) The resulting intensified electric currents generate complex magnetic fields which are the cause of a geomagnetic storm.

(5) Part of electrons carrying the intensified currents collide with upper atmospheric atoms and molecules and are responsible for causing ionizations there, causing auroral phenomena.

(6) An increased potential drop associated with an enhanced power drives the F-layer ionization in the dayside to drift into the polar cap, causing major changes in the distribution of the ionization.

A geomagnetic/ionospheric storm and an auroral display are nothing but different manifestations of the intensified currents. The higher the power of the generator is, the higher is the current intensity, causing more intense geomagnetic disturbances and brighter auroral displays. This is why both a very intense geomagnetic/ionospheric storm and a great auroral display occur together.

Therefore, the prediction of geomagnetic/ionospheric storms and the aurora is reduced to predicting the power of the generator which depends on the solar wind speed V, the solar wind magnetic field B and its polar angle θ. The first task of this project is thus to develop a method to predict the above three quantities (V, B, θ) for the interplanetary shock wave/driver gas and for an intense solar wind flow from a coronal hole.

In section 2, we describe the progress we have made in predicting major geomagnetic storms, in particular our efforts to cooperate the interplanetary scintillation (IPS) observation. As we shall describe in more detail later, the IPS observation serves the purpose of checking the prediction at a midpoint between the sun and the earth. In section 3, we describe the progress we have made in predicting the 27-day recurrent geomagnetic storms. We show that this particular project is reduced to predict the geometry of the neutral line on the source surface of the sun on the basis of the observed neutral lines during the past Carrington rotation. Thus, much of our effort has been concentrated in understanding the magnetic fields on the source surface and their variations.

2. PREDICTION OF MAJOR GEOMAGNETIC STORMS AFTER INTENSE SOLAR ACTIVITY

The modern prediction scheme should be able to provide not only just the occurrence and the maximum intensity for a given storm, but also the time development of the storm. Since the intensity of a geomagnetic storm field at a given time can be expressed in terms of the geomagnetic indices, we must be able to predict the geomagnetic indices as a function of time (such as AE, Dst, K_p, etc.), namely AE(t), Dst(t), K_p(t) etc. Toward this goal, we have developed a three-step process; (see Akasofu and Fry (1986) and Figure 4).

2.1 STEP 1

STEP 1: On the basis of the observation of a particular solar flare, we determine the following parameters:

1. Time (UT), date of the occurrence
2. View longitude (E,W), latitude (N,S) of flare
3. Initial speed of the solar wind*
4. Area covered by the flare*

5. Duration

The quantities with * depend on the intensity of a flare and are given in Table 1.

Table 1: Conversion From Flare Importance and Brilliance to V_F and σ_F

Importance/Brilliance	V_F (km s^{-1})	σ_F (c)
0F	200	20
0N	300	30
0B	400	40
1F	400	30
1N	600	40
1B	800	50
2F	500	30
2N	800	50
2B	1200	70
3F	700	30
3N	1100	50
3B	1500	70
4F	800	40
4N	1200	60
4B	1600	80

Using the above solar flare parameters as the input, a computer program has been developed to predict the solar wind speed (V) and the magnitude (B) of the interplanetary magnetic field at the front of the magnetosphere as a function of time, namely V(t), and B(t). When a number of flares take place during a given period, they can be inputed successively into the program. This is often the case, when there are one or more very active regions on the solar disk.

STEP 2: The predicted values in the above enable us to estimate the total maximum power P_m generated by the magnetospheric interaction as a function of time.

$$P_m \text{ (Mwatts)} = 20\ V\ (\text{km/sec})\ B^2(\text{nT})$$

Note that P_m differs from P by eliminating $sin^4(\theta/2) \leq 1.0$.

STEP 3: On the basis of the empirical relationships between P and AE, P and Dst, P and K_p, etc., we predict the geomagnetic indices AE(t), Dst(t) and $K_p(t)$ as a function of time. There is also an empirical relationship between P and the cross-polar cap potential Φ_{pc}.

- Using AE(t), Dst(t) and $K_p(t)$ thus determined, some other important parameters can also be predicted:
- The diameter of the auroral oval can also be estimated from the predicted AE(t) and Dst(t), since an empirical relationship between the oval diameter and AE/Dst has been established.
- The distribution of the electron density in the polar ionosphere after storm onset can also be predicted as a function of time by knowing the diameter of the auroral oval and the cross-polar cap potential Φ_{pc}.

We have tested the program extensively by 'postdicting' many past major solar terrestrial events during the last ten years or so and calibrated the computer code (cf. Akasofu and Lee, 1988, 1989, 1990).

One of the difficulties we encountered in applying our prediction scheme is that a major active region on the sun produces many flares, more than 10 in a two-week period. Since not all flares produce interplanetary disturbances, it has been difficult from the flare observation alone to determine which flares are likely to have caused interplanetary disturbances.

GEOMAGNETIC STORM PREDICTION SCHEME

DATE, TIME	SOLAR WIND SPEED	AE (t)
LONGITUDE, LATITUDE	MAGNETIC FIELD MAGNITUDE	DST (t)
INITIAL SPEED	MAGNETIC FIELD POLAR ANGLE	KP (t)
AREA		OVAL SIZE
DURATION		IONOSPHERE

FIGURE 4

It is very fortunate that an analysis of the interplanetary scintillation (IPS) has now become available. In the IPS study, radio waves from a predetermined set of radio galaxies and quasars are monitored by a fixed antenna system or systems. Thus, if a plasma cloud ejected by a solar flare is located between a radio galaxy and the earth, a strong scintillation of the radio wave from the radio galaxy is observed (Figure 5). The fixed antenna system can scan the entire sky, as the sky 'rotates' around the earth. Since the plasma cloud covers only a portion of the sky, the IPS region occupies only a limited region in the sky (the sky map). Therefore, we have modified our computer code to produce predicted IPS sky maps which indicate portions of the sky where IPS is expected to occur for a given flare.

In this way, we can compare the observed sky map and the predicted sky map during the transit of the plasma cloud from the sun to the earth. If there is any major disagreement between them, we can modify the input flare parameters until both agree. The steps to be taken in this scheme are graphically illustrated in Figure 6.

(i) Determine the six parameters from the observation of a flare.

(ii) Using the solar wind code, determine the geometry of the shock front at predetermined hours after the flare. The predetermined hour depends on the location(s) of the IPS observation.

(iii) Project the computer geometry of the shock wave in the sky map.

(iv) Compare the sky map thus produced with the observed IPS sky map.

(v) If both sky maps agree, extend the computation on the basis of the same six parameters and compute V and B and then power P.

(vi) If the two sky maps are substantially different, change the six parameters or choose a different flare.

(vii) Repeat the process (vi) until the two maps agree reasonably well.

(viii) On the basis of the six parameters thus determined finally, compute V and B and then P_m.

Thus, it is our finding that the IPS observation can provide us with a valuable mid-point calibration in the storm prediction scheme. The IPS observation is found to be far more useful than a single space probe because we can infer a 3-D geometry of the expanding solar plasma cloud.

Since the present IPS observation uses a fixed antenna system, the sky can be 'scanned' only once a day at a station (using the earth's rotation). At the present time, IPS observations are conducted at two locations, Cambridge (England) and Nagoya (Japan). Thus, we can make the 'IPS calibration' about twice during the transit of the solar plasma cloud from the sun to the earth. Our prediction scheme has been developed to be able to produce expected IPS sky maps at any given time at both locations. It is learned that India will also soon join in the IPS observation.

We have tested the geomagnetic storm prediction scheme by including the IPS observations and found that the IPS observation can increase considerably the accuracy of the prediction (Akasofu and Lee, 1989, 1990).

In order to test the usefulness of IPS observations, we examined possible shock waves (in terms of time variations of the solar wind speed, the arrival time, etc.) which should have been caused by some of the seven flares during the period between September 21 and 27, 1978, by taking into account their location on the solar disk and their intensity. The coronal hole was also modeled carefully in order to account for the observed variations of the solar wind speed for the period between 22 September and 6 October. Since these interplanetary events tend to superpose upon each other, the speed, arrival time and intensity of a particular shock event cannot be investigated without considering all responsible flares and high speed streams. A quantitative method is needed to identify solar flares

which are responsible for the observed interplanetary events. The method we have developed is capable of handling several solar events.

It is after a large number of trials and errors that we have tentatively identified the cause-effect relationship between the flares and the interplanetary events during the period of our concern (Table 2). We have identified F1 on 21 September as the cause of the shock wave which was observed on 25 September at the Earth. However, this identification is not in agreement with that made by Cane et al. (1982). Thus, based on their conclusion, we repeated the modeling by assuming that F2 on 23 September is the cause of the shock wave on 25 September. The former modeling is called here Case 1 and the latter Case 2 (see Table 2). Table 3 shows the six parameters for the chosen flares, F1 (Case 1), F2 (Case 2), F3 and F6. It is assumed in this study that the background solar wind stream without the high speed stream is 350 km/sec. This is a reasonable choice based on the observations during this period.

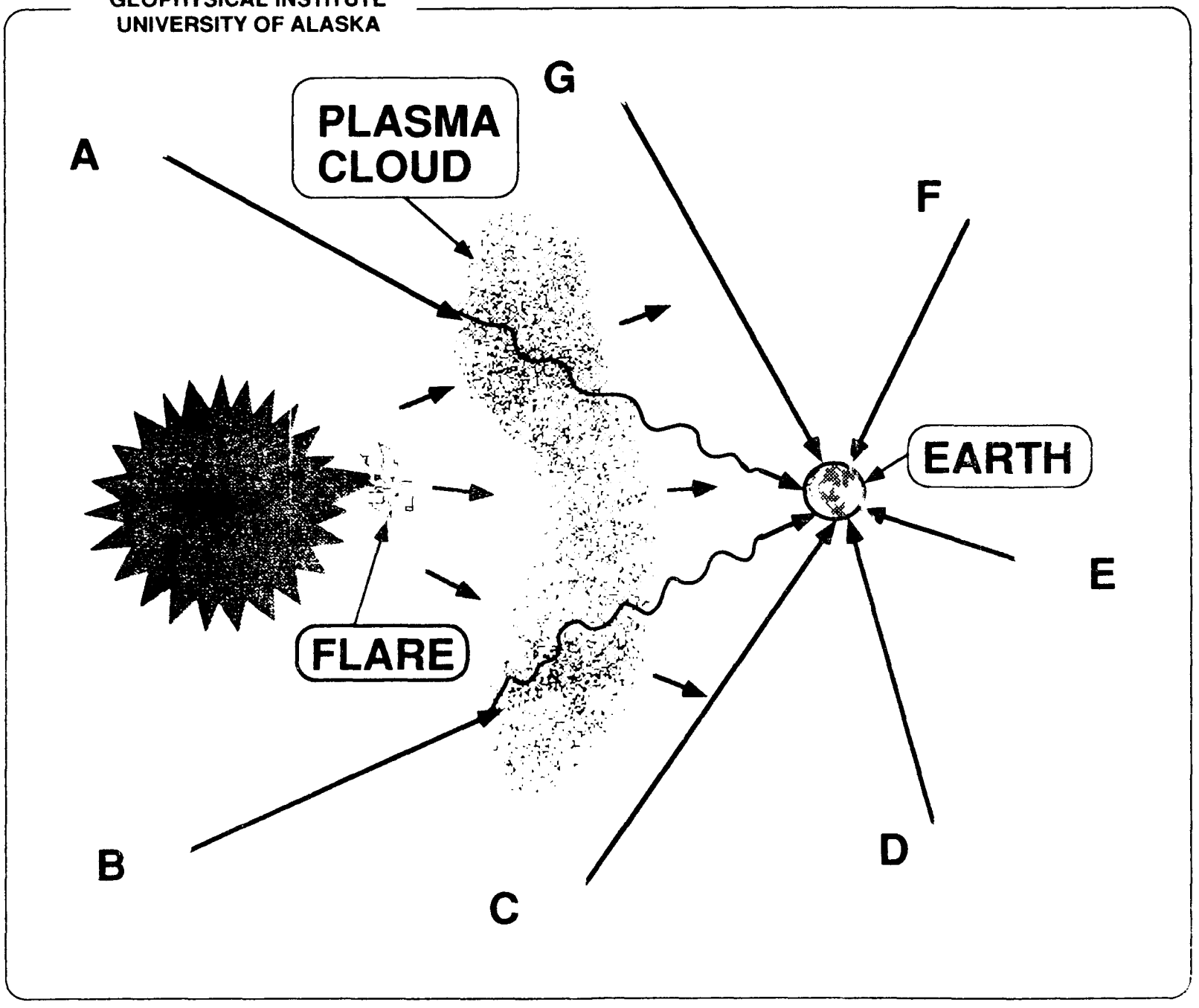
GEOPHYSICAL INSTITUTE
UNIVERSITY OF ALASKA
PLASMA CLOUD
G
A
F
EARTH
E
FLARE
B
C
D

FIGURE 5

NUMERICAL SCHEME ⇄ INTERPLANETARY SCINTILLATION (IPS) OBSERVATION

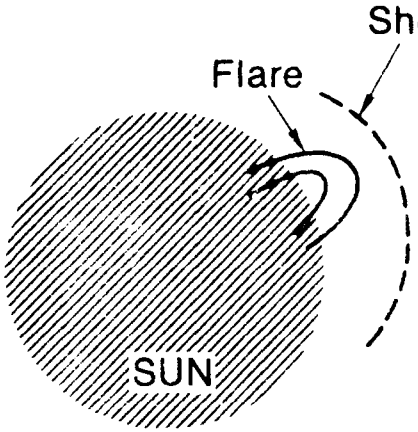

T = 0 Flare
(six parameters)

Numerical Scheme

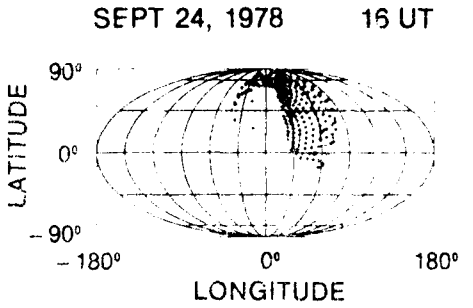

Predicted IPS Sky Map at T = 24 Hrs.

INTERPLANETARY SCINTILLATION

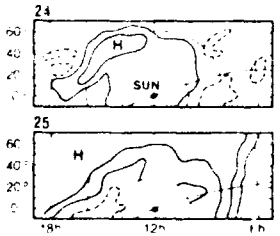

(Hewish et al, 1985)

SEPTEMBER, 1978

Observed IPS Sky Map at T = 24 Hrs.

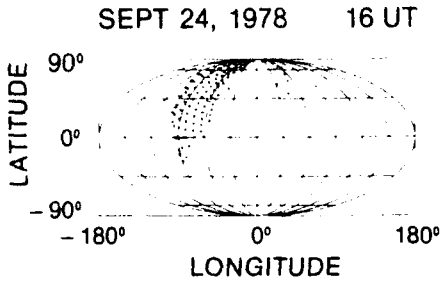

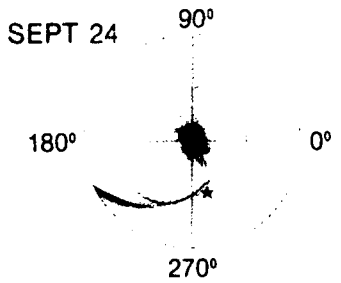

Improved Predicted Sky Map
(New six parameters at T = 24 Hrs.)

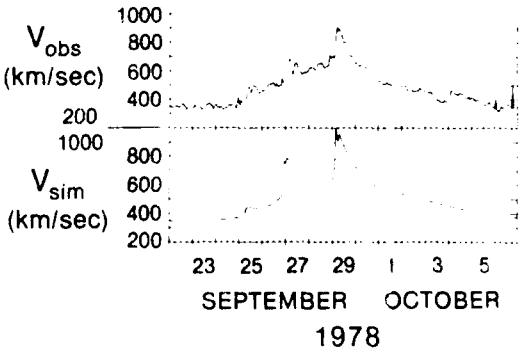

MODELING OF A SERIES OF INTERPLANETARY DISTURBANCE EVENTS

FIGURE 6

Table 2: List of Solar Flares Which Occurred Between 21 and 27 September 1978: Among Them F1, F3 and F6 are Identified to be Responsible for S1, S2 and S3, Respectively.

Flares	Interplanetary shock waves (arrival date and time)
F1: 21 Sept: 04:16 U.T.; N23 E40; 1B	Case 1-S1. 25 Sept: 01:16 U.T.
F2: 23 Sept: 09:44 U.T.; N35 W50; 3B	Case 2-S1: 25 Sept: 01:18 U.T.
F3: 24 Sept: 17:20 U.T.; N25 W07; 1B	S2: 26 Sept: 20:10 U.T.
F4: 24 Sept: 21:12 U.T., S20 W43; 2B	
F5: 27 Sept: 07:25 U.T.; S18 W80; 1F	
F6: 27 Sept: 08:18 U.T.; N10 W16; 1N	S3: 29 Sept: 03.01 U.T.
F7: 27 Sept: 14:28 U.T.; N27 W19; 2B	

Table 3: Parameters Employed for the Three Flares

Onset Time	Lat. Long (^{o},^{o})	V (km/sec)	τ (h)	σ (^{o})
Case 1 F1:21 Sept, 04:16, 1978	N23 E40	200	5.0	40
Case 2 F2:23 Sept, 09:44, 1978	N35 W50	2800	2.0	40
F3:24 Sept, 17:20, 1978	N25 W07	340	2.0	50
F6:27 Sept, 08:18, 1978	N10 W16	550	2.0	50

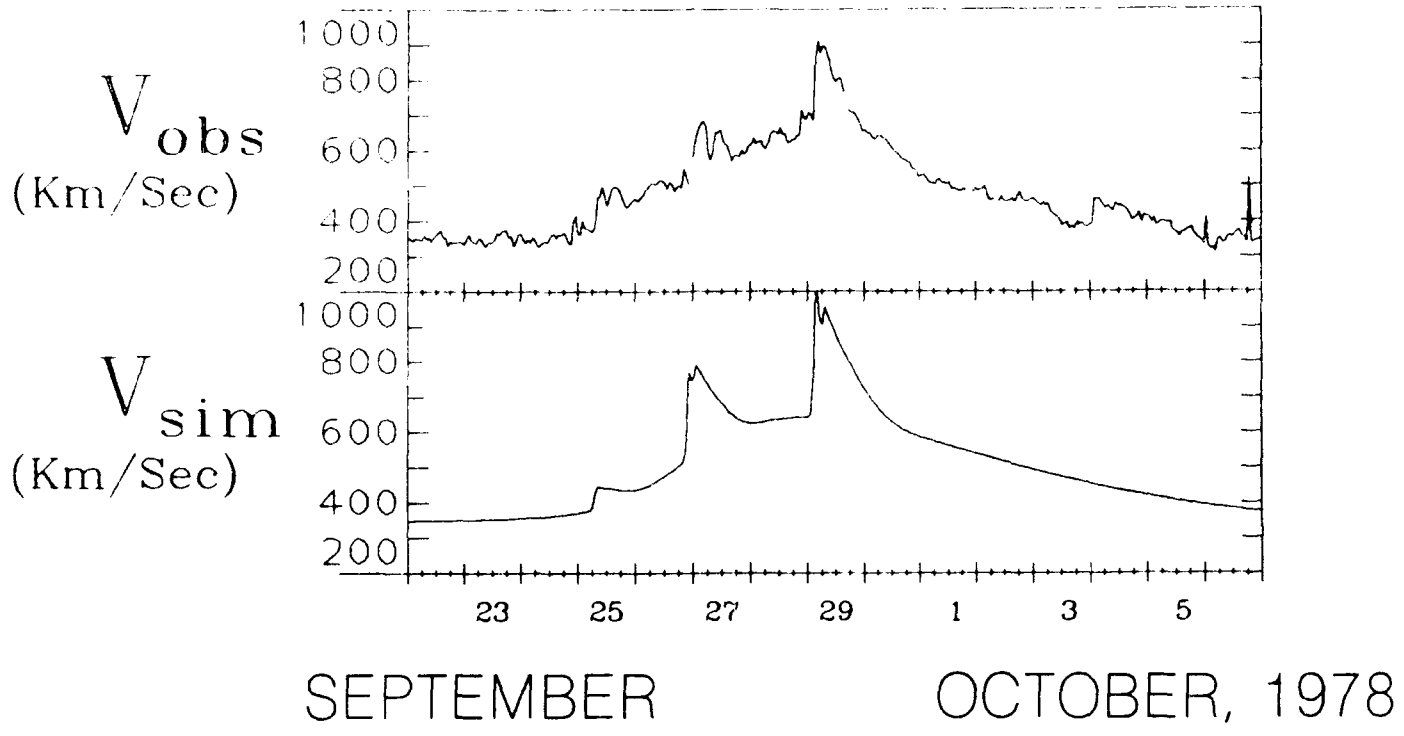
V_{obs}
(Km/Sec)
1000
800
600
400
200
V_{sim}
(Km/Sec)
1000
800
600
400
200
23
25
27
29
1
3
5
SEPTEMBER
OCTOBER, 1978

FIGURE 7a

Case 1

Figure 7a shows both the observed and the simulated variations of the solar wind speed. The results are obviously not totally satisfactory. However, this is the best fit obtained by our method. A change of any one of the parameters affects overall results in very complicated ways, because the observed results are a superposition of individual events. For example, if the simulated peak speed of the solar wind on 29 September is reduced, in order to make a better fit with the observation, its arrival time will shift from the observed one, as well as the speed and arrival time of all the other shocks. Thus, the identification of the responsible flare (F6) becomes questionable. However, it was found that the other flares give a worse fit than F6. A better fit would also be made by adjusting the speed of the high speed stream. However, such a change affects the overall variations of the solar wind speed during the entire period, resulting in often different combinations of the cause (flare)-effect (shock) relationship which is worse than what we have obtained so far. At this stage of development in this study, a better fit between the observation and the simulation is difficult without additional observations for the identification.

The three-dimensional structure of the expanding shock wave caused by F1 is shown in Figure 7b. Note that the second shock wave generated by F2 begins to appear on 25 September; both the longitude and latitude lines of interval 5^0 are used to provide the geometry of the shock wave. The shock associated with the IPS event reached the Earth on 25 September. The corresponding IPS sky maps are also constructed on the basis of Fig. 7b and are shown in Fig. 7c. The crosses indicated cross points of the latitude and longitude lines with 5^0 intervals. From Fig. 7c, one can see that the shock wave covered almost one half of the sky centered around the Sun (although the 5^0 interval mesh is too coarse to show the shock in the vicinity of the center of the sky map when it is too close to the Earth).

Indeed, the IPS observation showed that this was indeed the case (Tappin et al., 1983; a part of Fig. 2 in Hewish et al. (1985) is reproduced here as Fig. 7d. In particular, note that the highest IPS occurred in the 30°-60°E sector, centered around latitude 50°N. Our results (Figure 7c) are in good agreement with the observed IPS distribution (Figure 7d).

Case 2

It is natural to try to associate interplanetary events with most intense activities on the Sun. during the period of our concern, there occurred a 3B flare (F2) (N35, W50) at 09:44 U.T. on 23 September; see Table 2. It has been generally believed that the second interplanetary shock event (S2) at 20:10 U.T. on 26 September was caused by this 3B flare. However, this association requires an average speed of the shock wave of about 920 km/sec (Cane et al. 1982, 1986; Cane and Stone, 1984). One difficulty we face here is that the solar wind speed at the time of the arrival of S2 was only about 400 km/sec and the estimated initial speed was more than 2500 km/sec (Cane et al., 1982). Thus, it was difficult to model F2 as the flare responsible for S2.

In spite of such difficulties, we have attempted to model the possible association between F2 and S1 by choosing the parameters listed in Table 3. The corresponding results show that the computed IPS disagrees with the observed one. In this case, the computed IPS was mostly confined to the western sky, while the observed one was in the eastern sky (as discussed in Case 1).

2.2 STEP 2

The STEP 2 is simply to compute the maximum power P_m as a function of V and B which are computed in STEP 1. The power P thus determined is a function of time.

Sept. 22

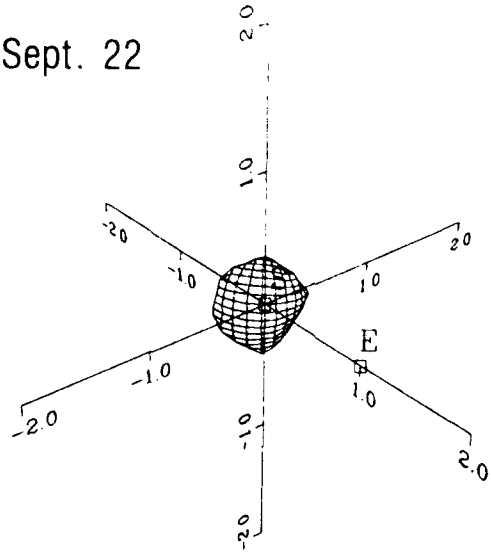

Sept. 23

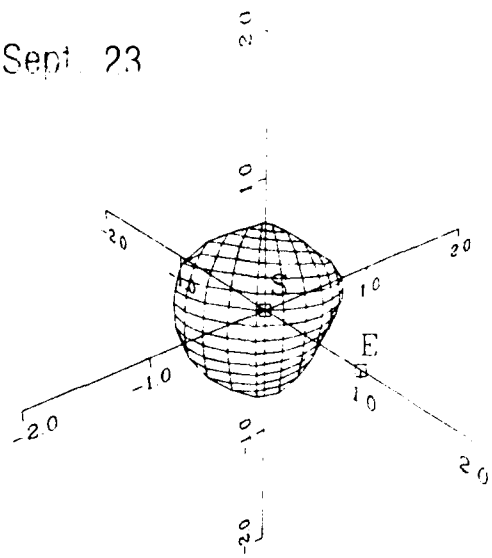

Sept. 24

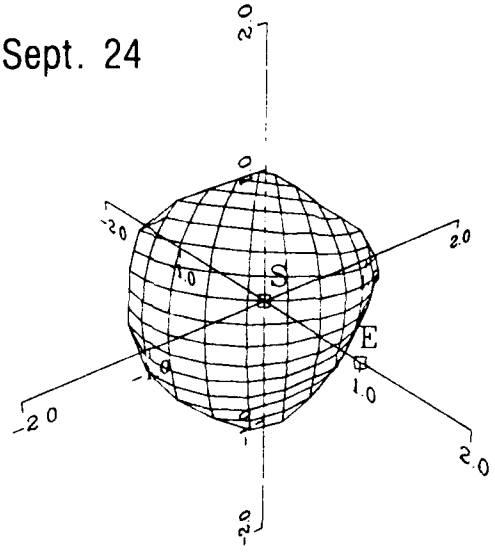

Sept. 25

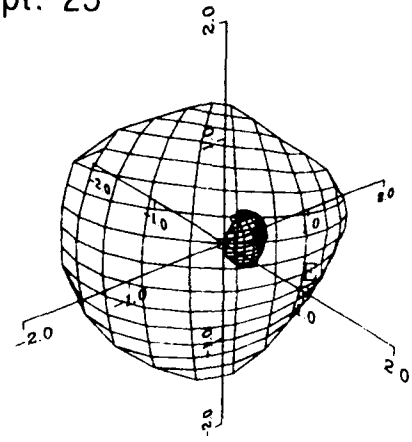

Sept. 26

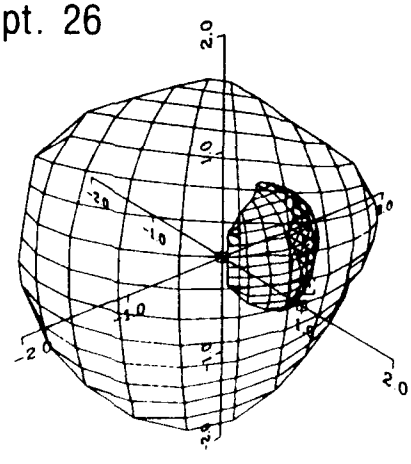

Sept. 27

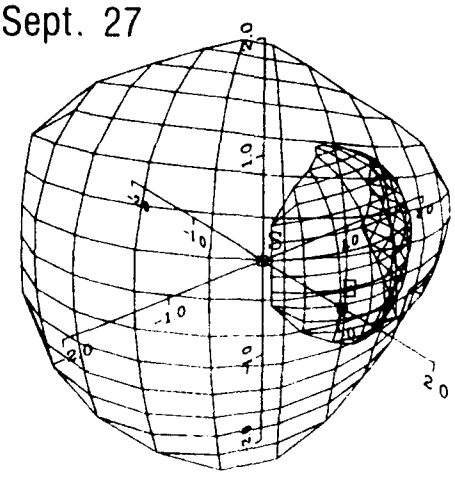

SEPTEMBER, 1978

FIGURE 7b

SEPT 22, 1978
16 UT

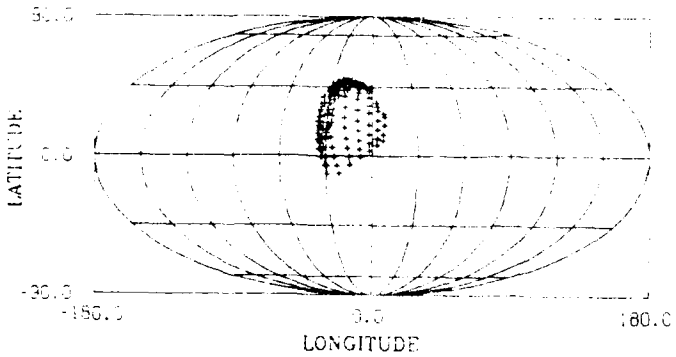

SEPT 23, 1978
16 UT

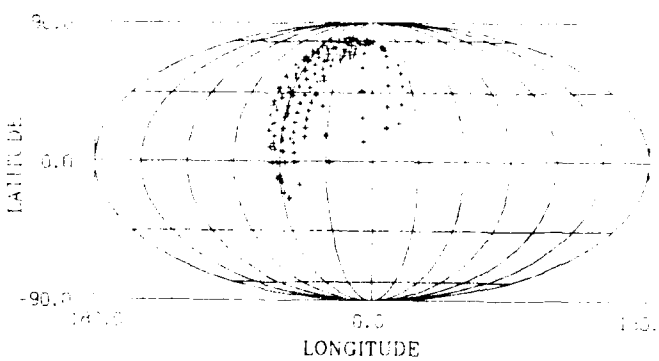

SEPT 24, 1978
16 UT

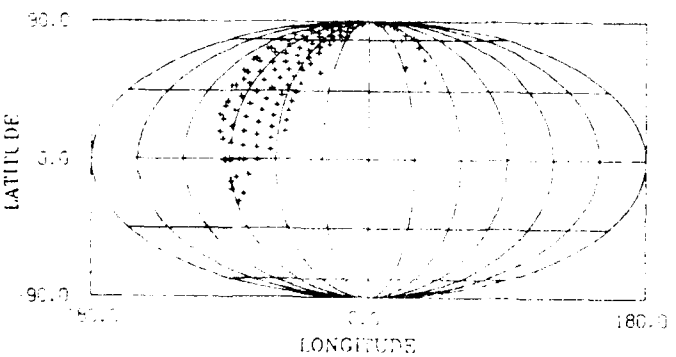

SEPT 25, 1978
16 UT

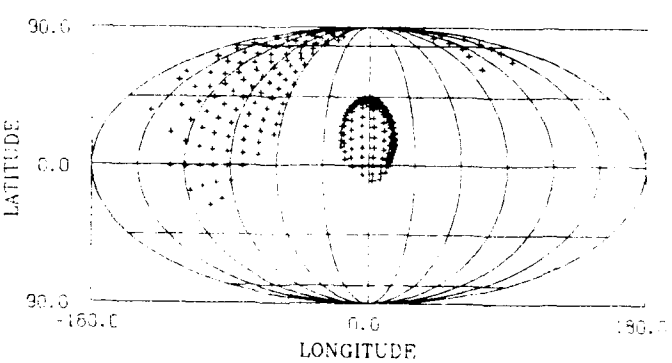

SEPT 26, 1978
16 UT

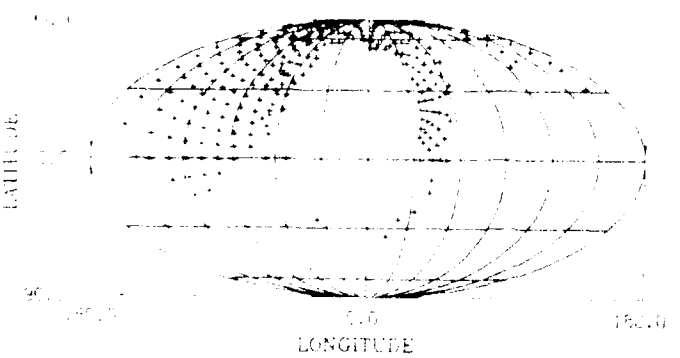

SEPT 27, 1978
16 UT

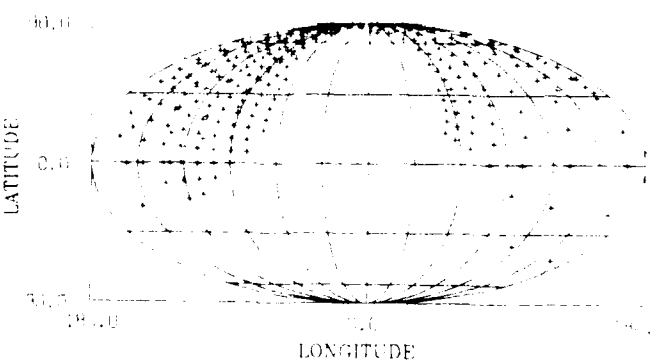

FIGURE 7c

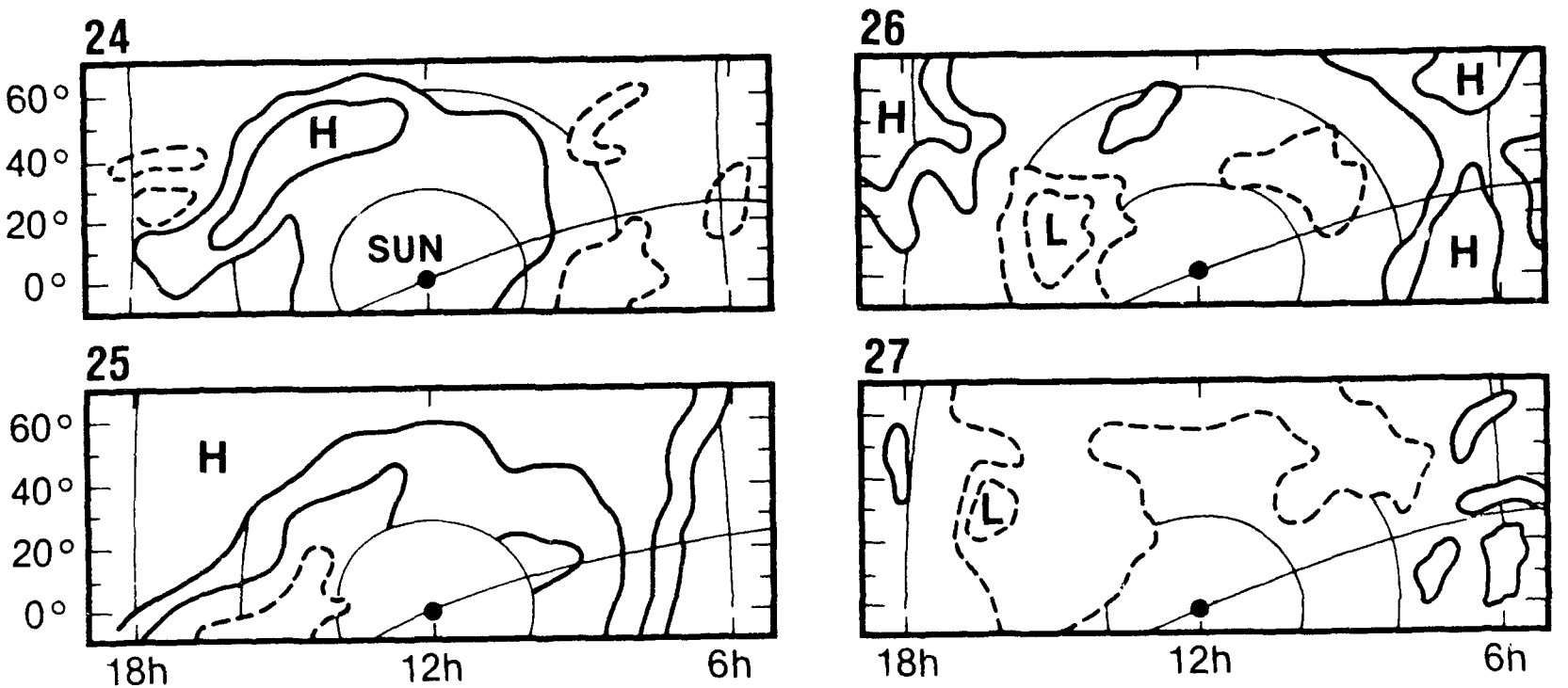
INTERPLANETARY SCINTILLATION
24
26
25
27
60°
40°
20°
0°
H
SUN
L
18h
12h
6h
(HEWISH et al 1985)
SEPTEMBER, 1978

FIGURE 7d

2.3 STEP 3

(a) *Geomagnetic Indices*

There is no theory to relate directly the power P of the solar wind-magnetosphere dynamo to the geomagnetic indices AE, Dst, Kp, etc. However, there are empirical relationships between P and AE, P and Dst, etc.

$$AE(nT) = -300 (\log P)^2 + 11800 \log P - 113200$$

$$|Dst\ (nT)| = 60 (\log P - 18)^2 + 25$$

Thus, both AE and Dst can be computed as a function of time when P is given as a function of time. Since the present prediction scheme can provide P_m, instead of P, we can estimate only the maximum possible AE and Dst by replacing P by P_m.

(b) *Cross-Polar Cap Potential* Φ_{pc}

Reiff et al. (1981) found that the polar cap potential Φ_{pc} is related to the Power P by $\Phi_{pc} = (0.93P - 319)^{1/2}$. Thus, it is possible to predict Φ_{pc} as a function of time if P can be predicted. Since we can predict P_m, we shall be able to predict maximum values of Φ_{pc}.

(c) *Equivalent Circuit*

One way to replace the empirical relationship between P and AE is to consider an equivalent current circuit. For this purpose, Liu et al. (1988) developed an equivalent circuit (a computer code) for the magnetosphere (Figures 8a and 8b). Once P(t) can be inferred from Steps 1 and 2 (Figure 1), it is possible to determine the input voltage Φ_{CT} for the circuit. The equivalent circuit can then determine all the magnetospheric quantities. Figure 8b shows how the magnetosphere responds to a step-function like increase of Φ_{CT}. The response as a function of time may be seen clearly in the cross-polar cap potential Φ_{pc} and the total energy deposition in the ionosphere (denoted by WB).

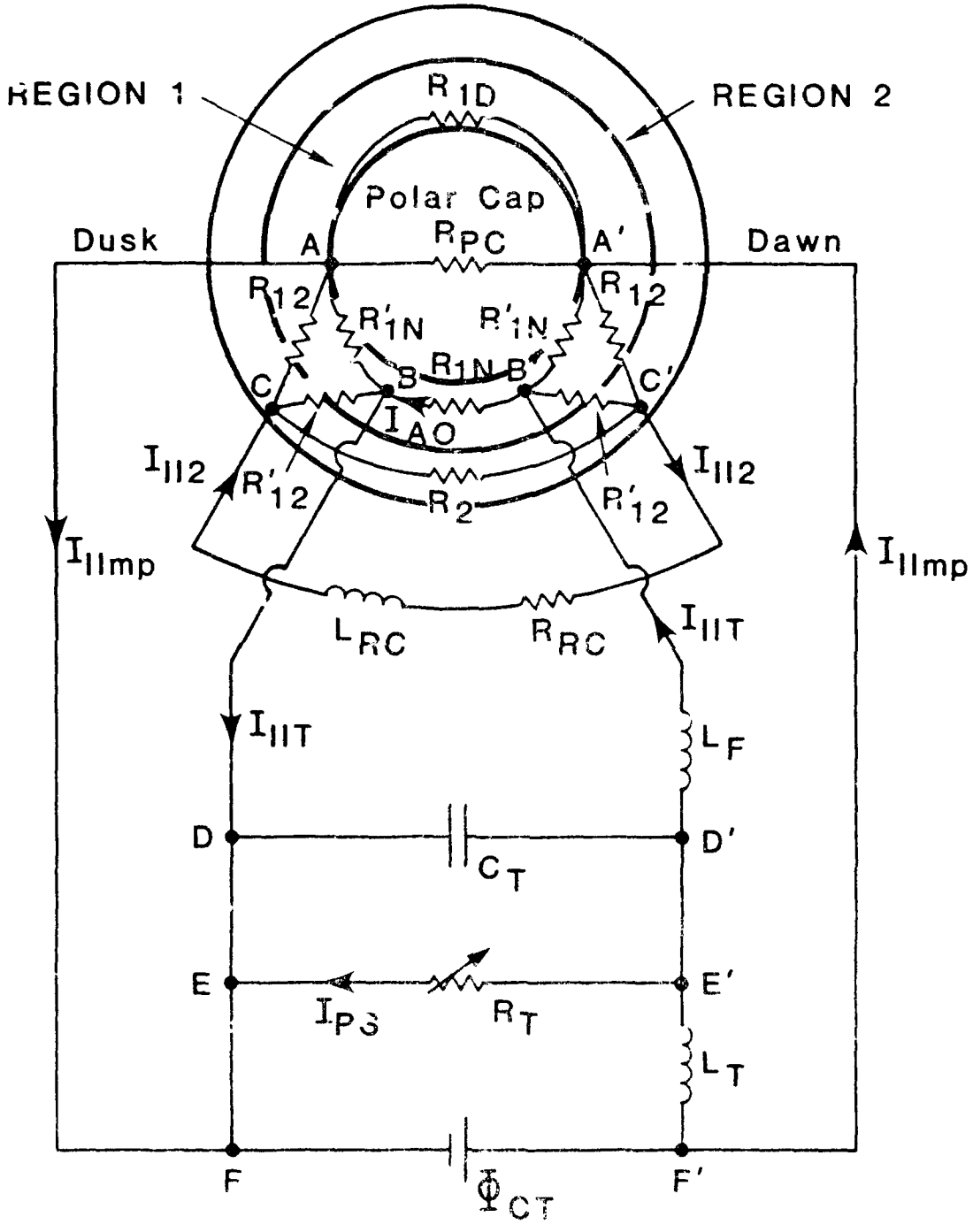
REGION 1
REGION 2
R_{1D}
Polar Cap
R_{PC}
Dusk
Dawn
A
A'
R_{12}
R_{12}
R'_{1N}
R'_{1N}
B
R_{1N}
B'
C
C'
I_{AO}
I_{II2}
R'_{12}
R_2
R'_{12}
I_{II2}
I_{IImp}
I_{IImp}
L_{RC}
R_{RC}
I_{IIT}
I_{IIT}
L_F
D
D'
C_T
E
E'
I_{PS}
R_T
L_T
F
F'
Φ_{CT}

FIGURE 8.

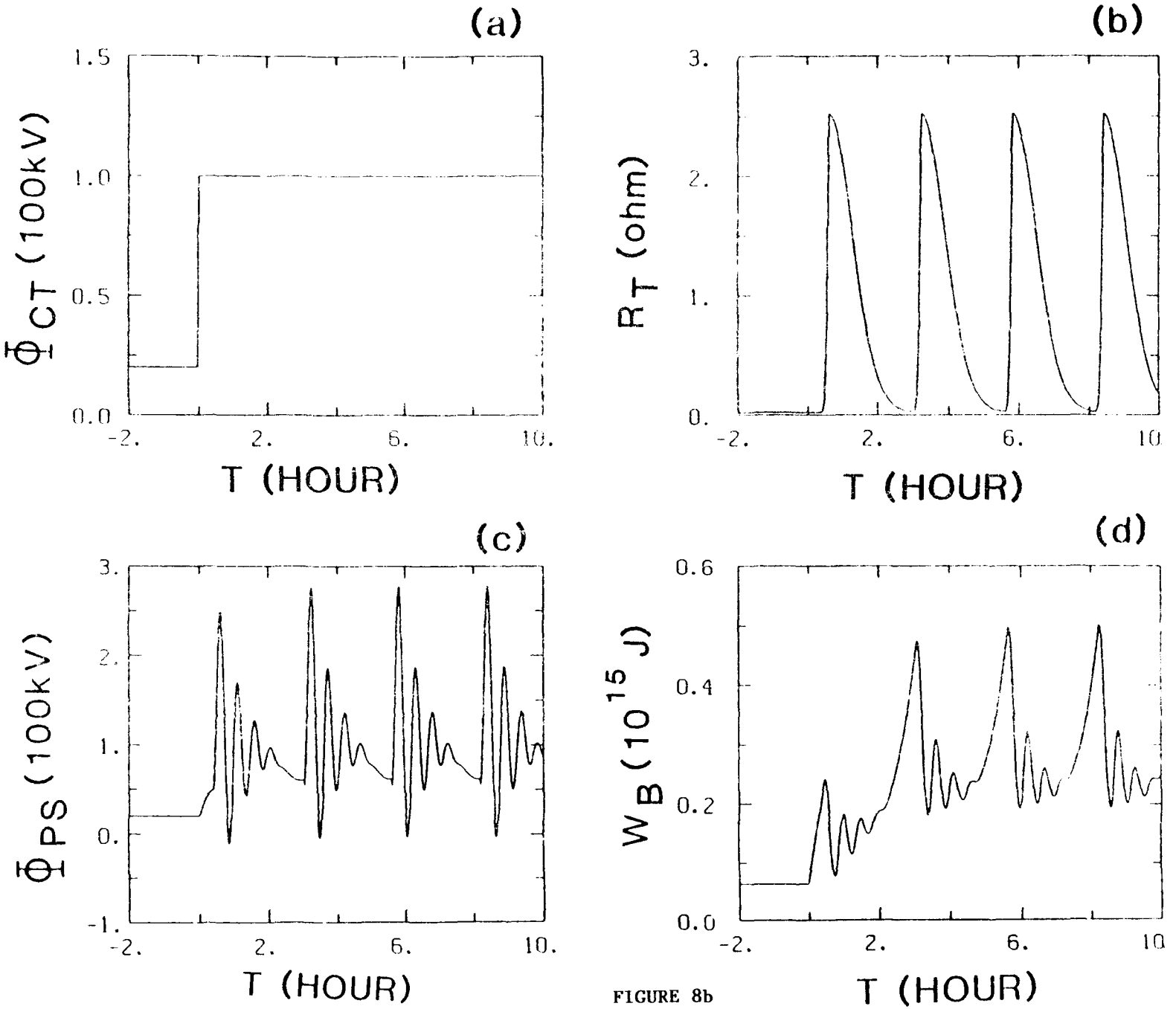
(a)
1.5
1.0
0.5
0.0
Φ_{CT} (100kV)
-2.
2.
6.
10.
T (HOUR)
(b)
3.
2.
1.
0.
R_T (ohm)
-2.
2.
6.
10
T (HOUR)
(c)
3.
2.
1.
0.
-1.
Φ_{PS} (100kV)
-2.
2.
6.
10.
T (HOUR)
(d)
0.6
0.4
0.2
0.0
W_B (10^{15} J)
-2.
2.
6.
10
T (HOUR)

FIGURE 8b

(d) Φ_{pc} *and AE*

Another important progress in this regard is that we have determined the relationship between the cross-polar cap potential drop Φ_{pc} and the AE index on the basis of both satellite-based and ground-based data (Akasofu et al. 1990). The results are shown in Figure 9. Since Φ_{pc} (Kv) = 36 + 0.89 AE or AE = 11.2 (Φ_{pc} -36), if the relationship between the solar wind quantities (V, B, θ) and the cross-polar cap potential can be established, it is possible to predict the AE index as a function of time.

(e) *Polar Ionosphere*

Once the cross-polar potential Φ (or Φ_{pc}) can be determined as a function of time, it is now possible to compute the electron density distribution as a function of time over the entire polar region. Figure 10 shows the computational scheme and Figure 11 shows an example of the results. One can see clearly that the ionization produced by the solar radiation in the dayside hemisphere is driven into the polar cap from the cusp region. In the polar region, however, there is also the ionization caused by the precipitation of auroral particles. This model reproduces fairly well the ionospheric trough. Note in particular that the trough extends from the night sector to the day sector, as discovered by Whalen (1989).

(f) *IMF Polar Angle* θ

An accurate determination of the power P requires not only V and B, but also the polar angle θ. Unfortunately, inspite of our efforts during the last several years, we are far from predicting θ as a function of time. So far, our prediction code can determine V and B, but not θ. Thus, we can simply estimate the maximum possible power P_m.

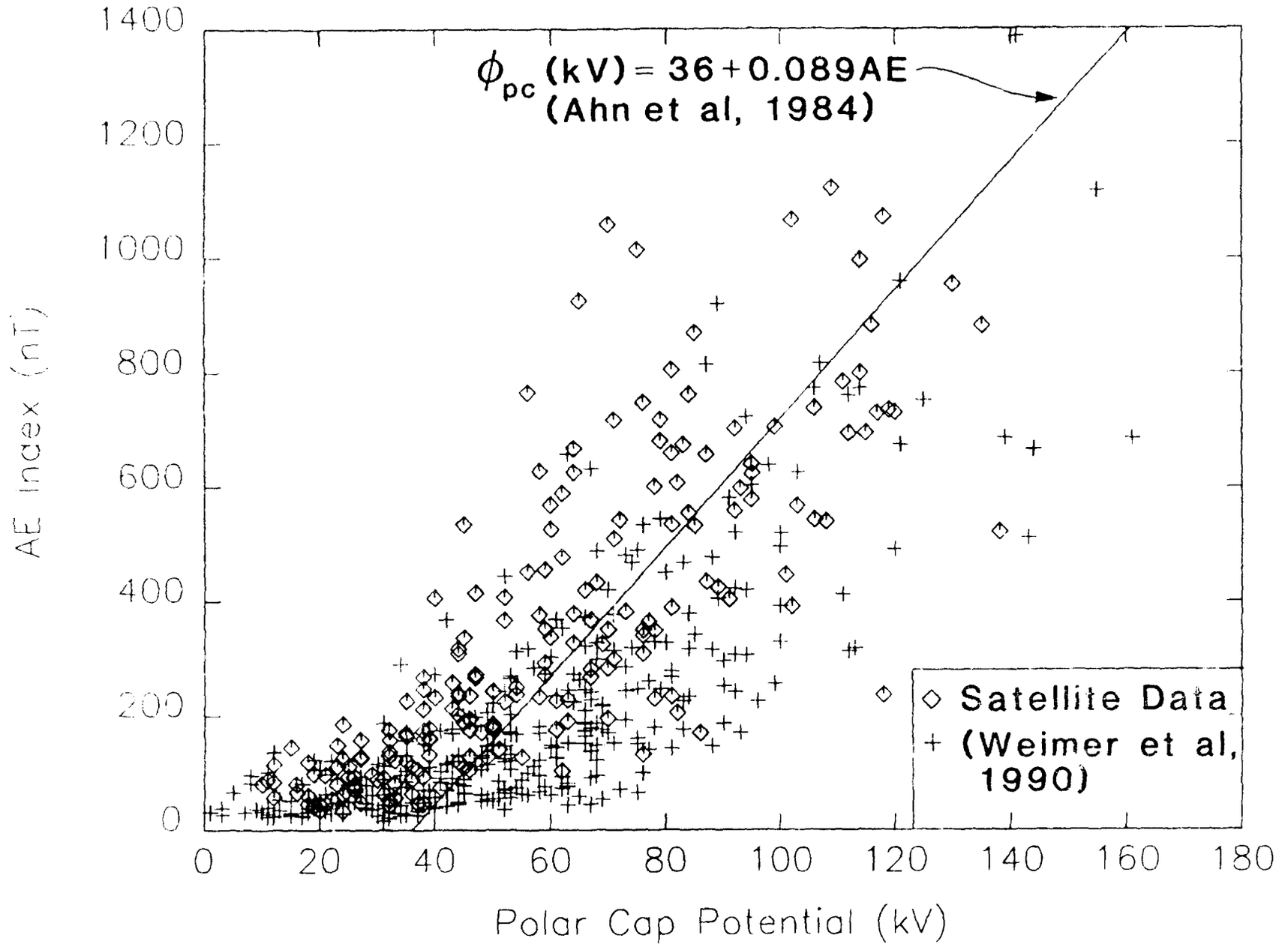
ϕ_{pc} (kV) = 36 + 0.089AE
(Ahn et al, 1984)
◇ Satellite Data
+ (Weimer et al, 1990)
AE Index (nT)
Polar Cap Potential (kV)
0
200
400
600
800
1000
1200
1400
0
20
40
60
80
100
120
140
160
180

FIGURE 9

IONOSPHERIC STORM PREDICTION

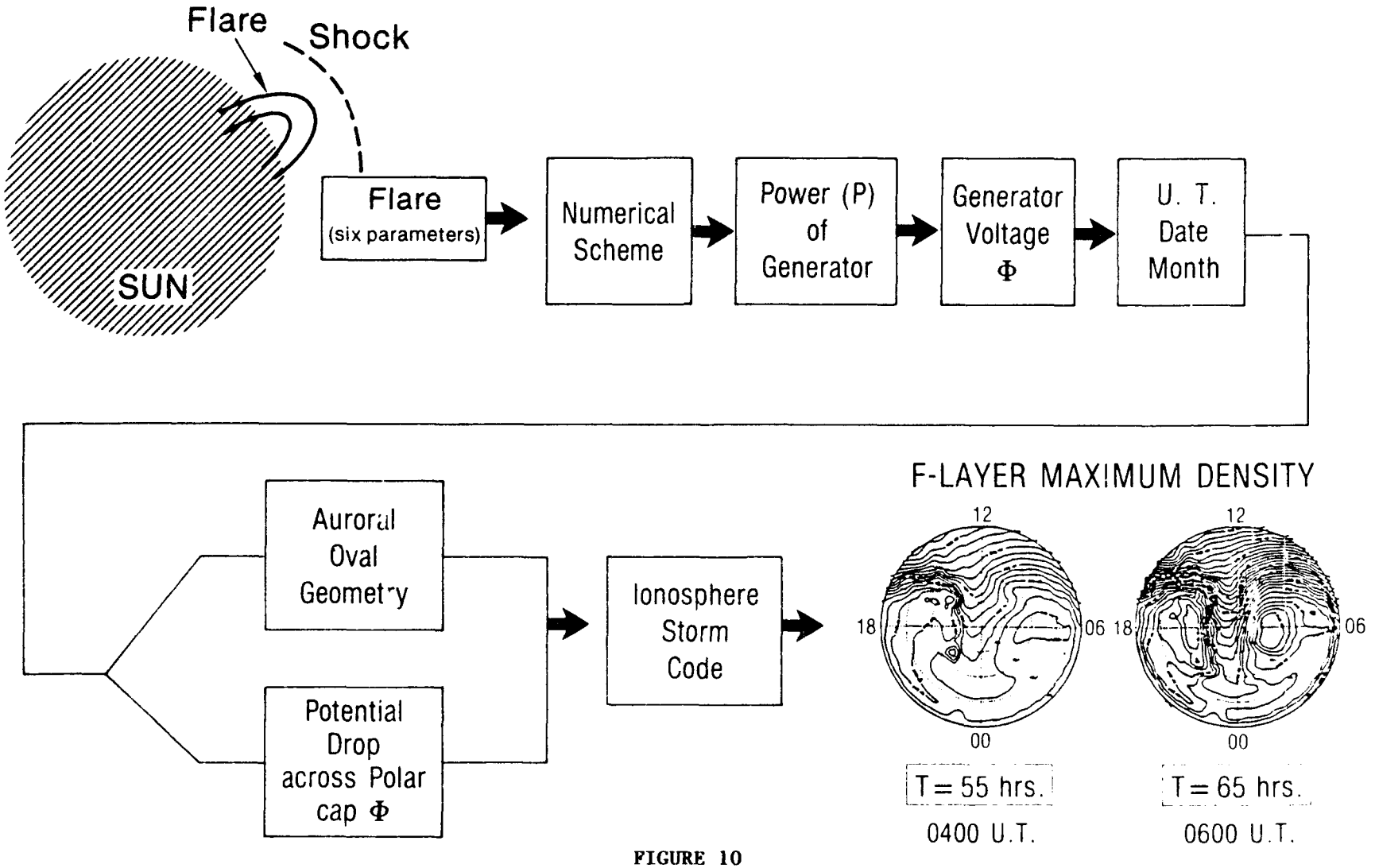

FIGURE 10

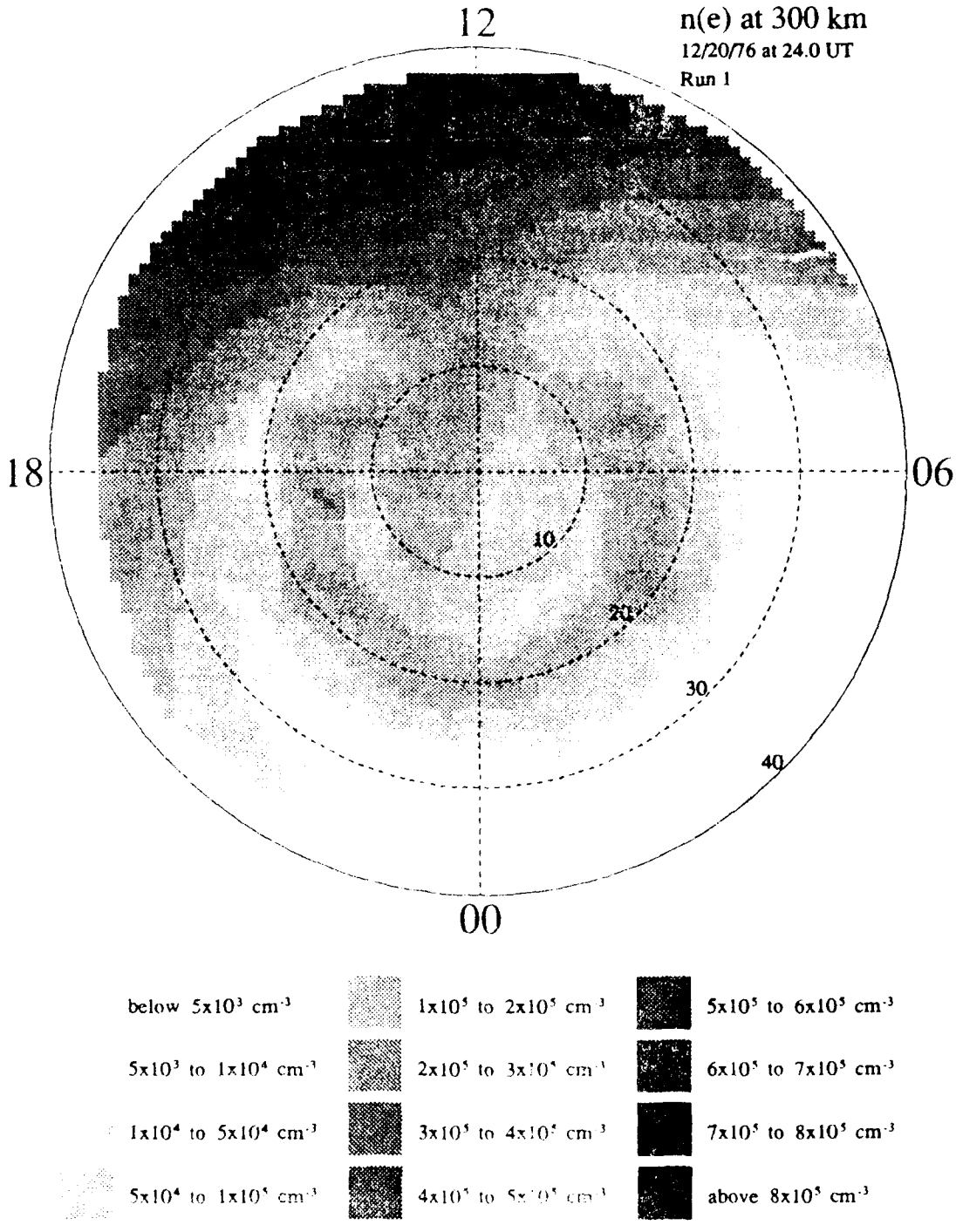
12
n(e) at 300 km
12/20/76 at 24.0 UT
Run 1
18
06
00
10
20
30
40
below 5x10³ cm⁻³
5x10³ to 1x10⁴ cm⁻³
1x10⁴ to 5x10⁴ cm⁻³
5x10⁴ to 1x10⁵ cm⁻³
1x10⁵ to 2x10⁵ cm⁻³
2x10⁵ to 3x10⁵ cm⁻³
3x10⁵ to 4x10⁵ cm⁻³
4x10⁵ to 5x10⁵ cm⁻³
5x10⁵ to 6x10⁵ cm⁻³
6x10⁵ to 7x10⁵ cm⁻³
7x10⁵ to 8x10⁵ cm⁻³
above 8x10⁵ cm⁻³

FIGURE 11

(a) $t = 0$ (b) $t = 3.41\ t_A$ (c) $t = 6.95\ t_A$

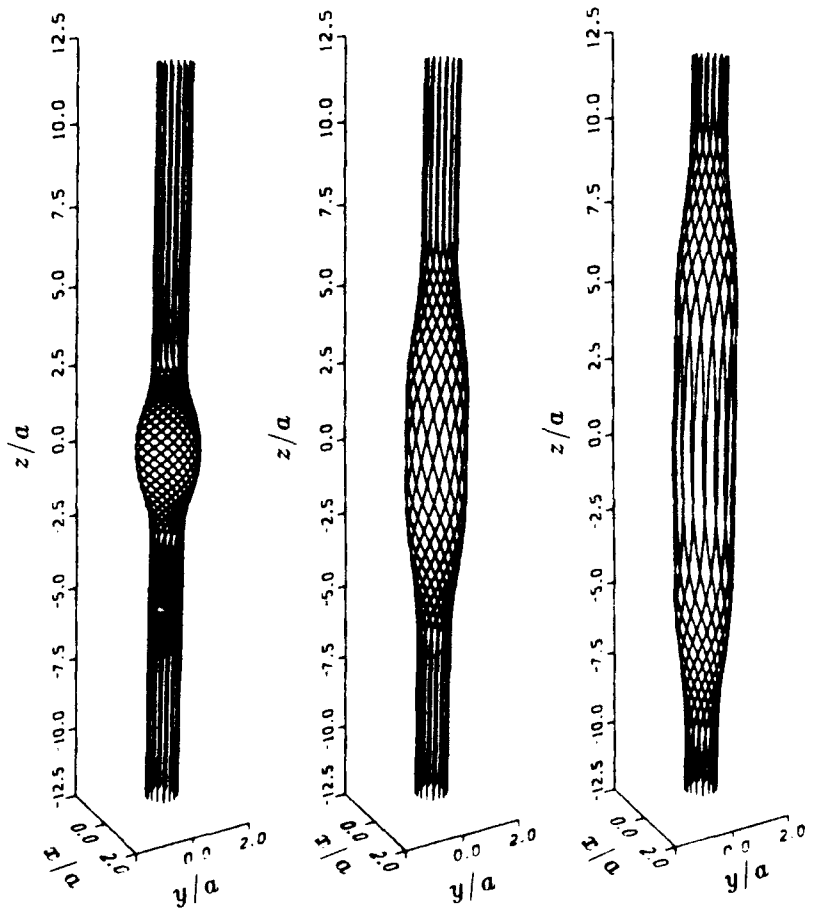

FIGURE 12a

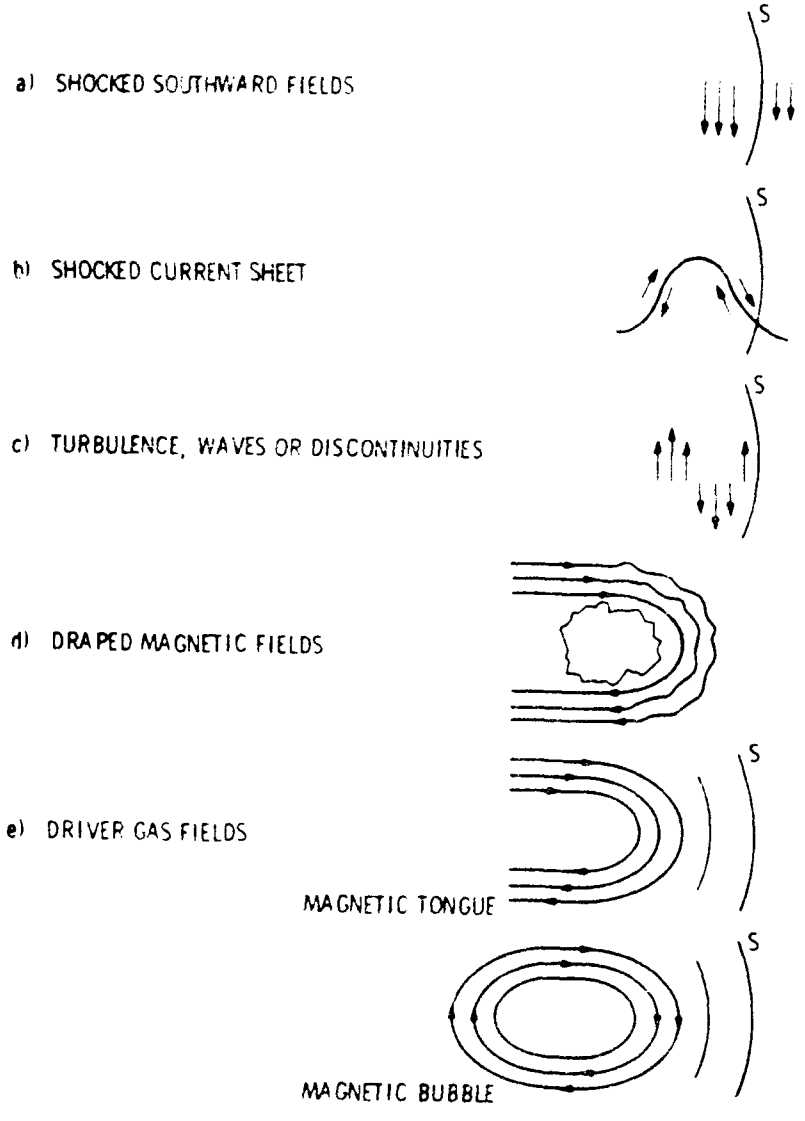
a) SHOCKED SOUTHWARD FIELDS
S
b) SHOCKED CURRENT SHEET
S
c) TURBULENCE, WAVES OR DISCONTINUITIES
S
d) DRAPED MAGNETIC FIELDS
e) DRIVER GAS FIELDS
S
MAGNETIC TONGUE
S
MAGNETIC BUBBLE

FIGURE 12b

In order to understand the magnetic field configuration in the driver gas, we have started to model a magnetic cloud. Figure 12a shows a study of the propagation of a "magnetic cloud" along a flux of the interplanetary magnetic field (IMF) lines (Wang et al. 1988; Wei et al. 1990). When the earth encounters such a structure, the IMF vector at the earth is expected to vary in a complicated way. Our study can, however, predict the expected type of variations in a magnetic cloud or a driver gas. It has been suggested that such a "magnetic cloud" is generated above a flare and propagate out in interplanetary space. So far, we have identified several causes for variations of θ (Figure 12b). However, we are unable, at the present time, to identify which causes dominate variations of θ for a given flare.

3. PREDICTION OF THE 27-DAY RECURRENT STORMS

3.1 Introduction

The past prediction method of recurrent geomagnetic/ionospheric storms is based on a study of the so-called "Bartels Kp musical diagrams." Obviously, such a method is not based on physics. Like flare-caused storms, the modern scheme must be based on the prediction of the power of the generator. Thus, the prediction of the 27-day recurrent geomagnetic storms is reduced to predict the power P for a 27-day period and the geomagnetic indices AE, Dst, Kp, etc. for the same period. At the present time, it is not known how Alfvén waves and turbulence are generated in a high speed stream. Thus, it is not possible to predict the polar angle θ. However, it is possible to predict the of $P = 20\ VB^2 \sin^4(\theta/2)$, namely $|P| = 20\ VB^2$, since $0 \leq \sin^4(\theta/2) \leq 1.0$. Then, from the envelope of P, it is possible to infer the envelope of the AE index, a rough trend of the maximum AE index as a function of time.

Figure 13 shows variations of the solar wind quantities during the period between June 25 and July 21, 1974. Compare the observed VB^2 and the AE index. We can see that the general trend of AE index variations during the 27-day period follows reasonably well that of VB^2. Note that fine time variations of the AE index represent individual substorm. Thus, we can predict the upper limit of the AE index and of its 27-day variations if we succeed in predicting V and B for a 27-day period.

3.2 Neutral Line on the Source Surface

In the above, we have demonstrated that the forecasting of the recurrent geomagnetic activity is reduced to predicting the solar wind speed V and the magnitude B of the IMF for a 27-day period. In turn, the prediction of V and B is reduced to inferring geometry of the neutral line on the source surface which is an imaginary spherical surface of radius 2.5 solar radii. The natural line varies in a very complicated way during a sunspot cycle (Figure 14a). For this purpose, we must find a simple way to reproduce the neutral line. Fortunately, we found that the neutral line on the source surface can be reproduced fairly accurately by a dipole at the center of the sun and a few dipoles on the photosphere (Saito, Oki, Olmsted and Akasofu, 1989). This finding has provided us with an opportunity to predict the geometry of the neutral line on the source surface by extrapolating time variations of the characteristics of the dipoles.

3.3 A New Method of Representing the Neutral Line

In order to reproduce the observed neutral line on the source surface, we assume the axial dipole at the center of the sun and a few dipoles near the equatorial plane of the photosphere (Figure 14b). In the upper left diagram, the observed neutral line for Carrington rotation 1666 is shown, while the upper right diagram shows its reproduction using our modeling method (Saito, Oki, Olmsted and Akasofu, 1989). In this particular example, the two dipoles are located in low

latitudes on the photosphere. One can see that our method reproduces fairly well the observed neutral line in the upper left diagram. The lower diagrams are spherical representations of the upper ones. The cross in the upper right diagram shows the view longitude of the spherical presentation.

3.4 Representation of Neutral Line Variations

Figure 15 shows how accurately we can reproduce the observed neutral line by a combined axial field (in the righthand side) and four dipoles located in low latitude, No. 1, 2, 3, and 4. During four solar rotations, from Carrington rotation 1661-1664, the four dipoles varied rather fairly smoothly. Figure 16 shows time variation of the dipole No. 3 in terms of latitude, longitude, the azimuth and the magnitude. Thus, time variations of the equatorial dipoles can be extrapolated, allowing us to predict the geometry of the neutral line, in turn the solar wind speed V and the IMF magnitude B and finally the envelope of the maximum variations of VB^2 and of the AE index.

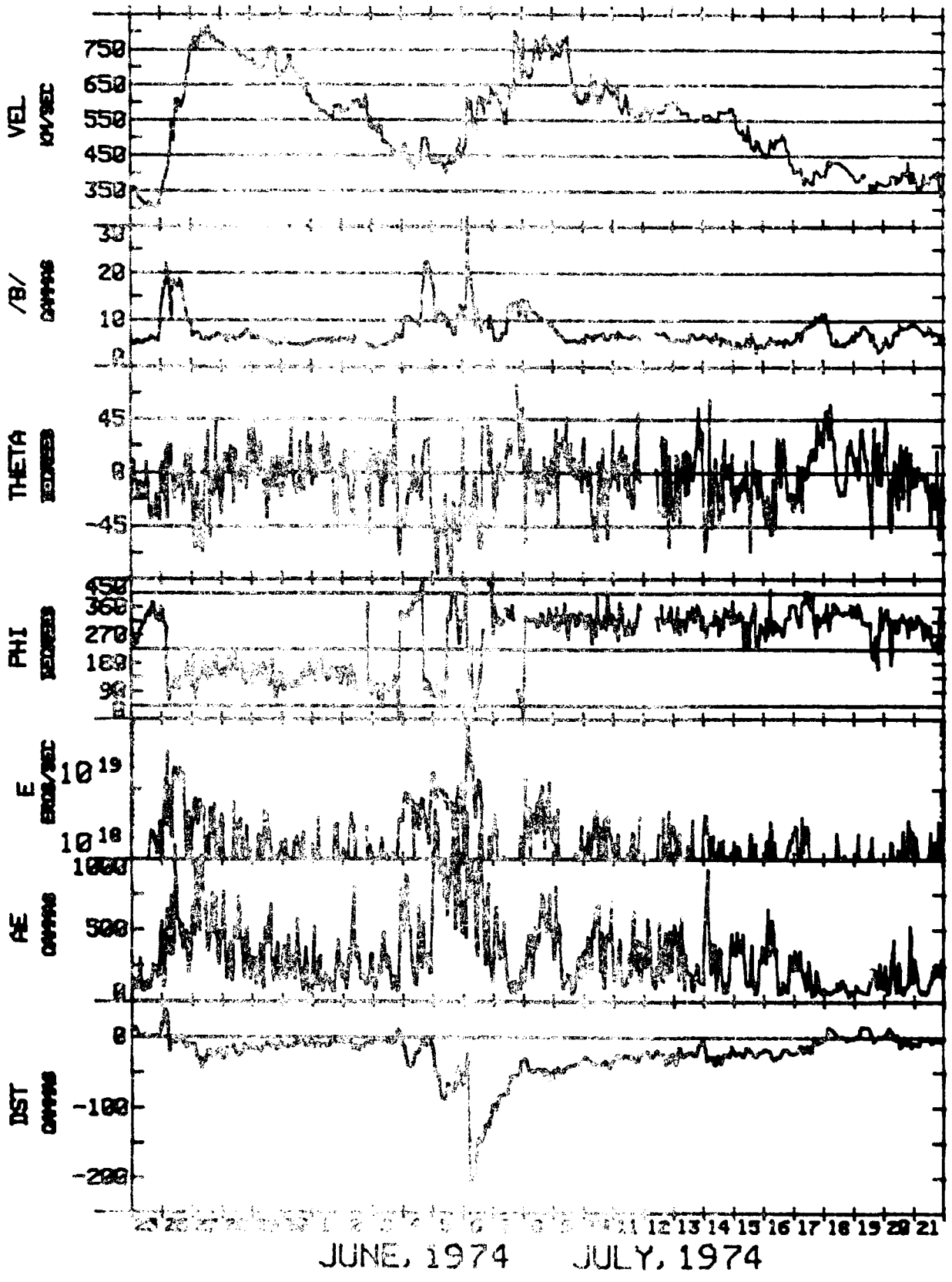
VEL
KM/SEC
750
650
550
450
350
/B/
GAMMAS
30
20
10
0
THETA
DEGREES
45
0
-45
PHI
DEGREES
450
360
270
180
90
0
E
ERGS/SEC
10^{19}
10^{18}
AE
GAMMAS
1000
500
0
DST
GAMMAS
0
-100
-200
20 21 1 2 3 4 5 6 7 8 9 10 11 12 13 14 15 16 17 18 19 20 21
JUNE, 1974
JULY, 1974

FIGURE 13

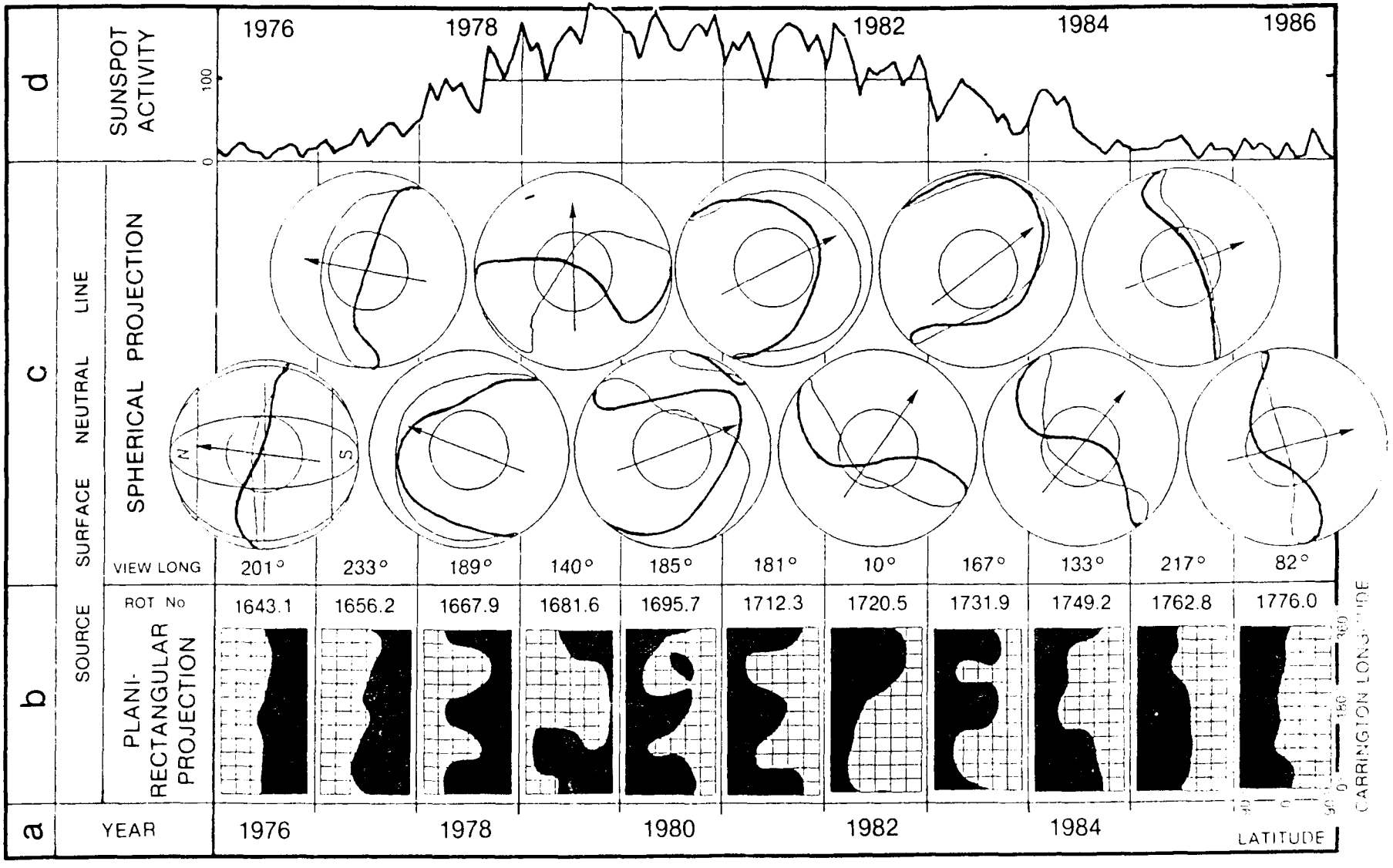
d
SUNSPOT ACTIVITY
1976
1978
1982
1984
1986
100
0
c
SURFACE NEUTRAL LINE
SPHERICAL PROJECTION
N
S
VIEW LONG
201°
233°
189°
140°
185°
181°
10°
167°
133°
217°
82°
b
SOURCE
ROT No
1643.1
1656.2
1667.9
1681.6
1695.7
1712.3
1720.5
1731.9
1749.2
1762.8
1776.0
PLANI-RECTANGULAR PROJECTION
CARRINGTON LONGITUDE
LATITUDE
a
YEAR
1976
1978
1980
1982
1984

FIGURE 14A

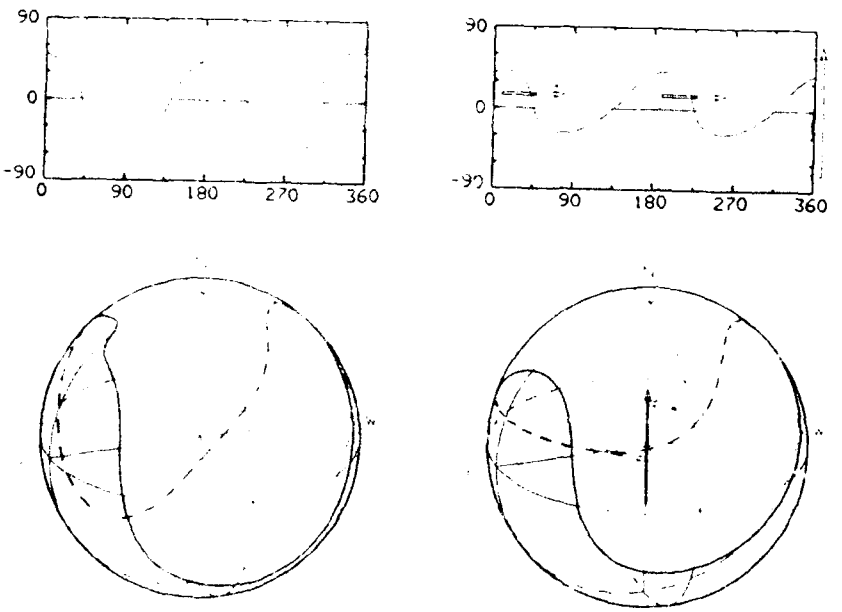

C.R. 1666

FIGURE 14b

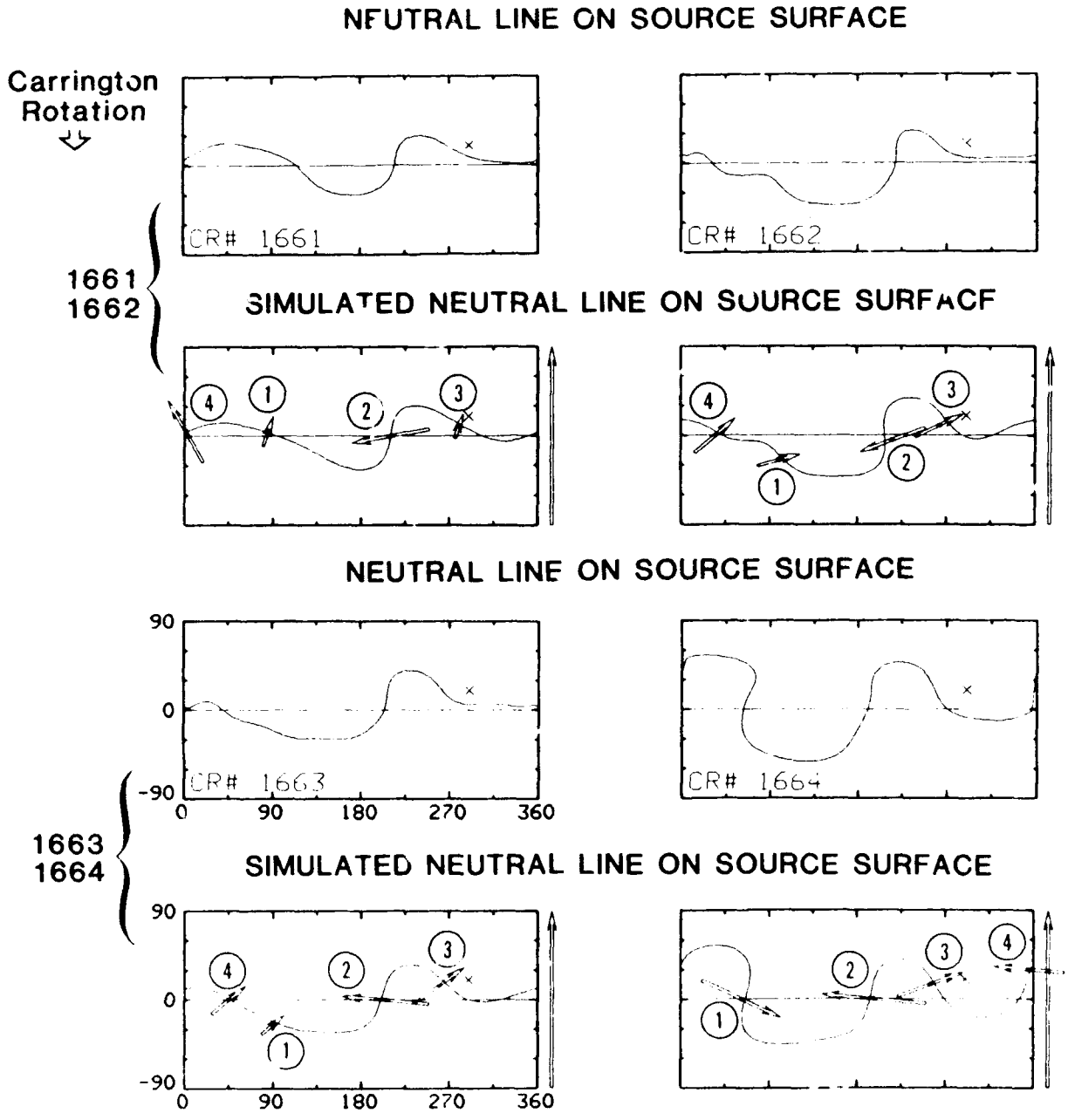
NFUTRAL LINE ON SOURCE SURFACE
Carrington Rotation
CR# 1661
CR# 1662
1661
1662
SIMULATED NEUTRAL LINE ON SOURCE SURFACE
NEUTRAL LINE ON SOURCE SURFACE
90
0
-90
CR# 1663
CR# 1664
0
90
180
270
360
1663
1664
SIMULATED NEUTRAL LINE ON SOURCE SURFACE

FIGURE 15

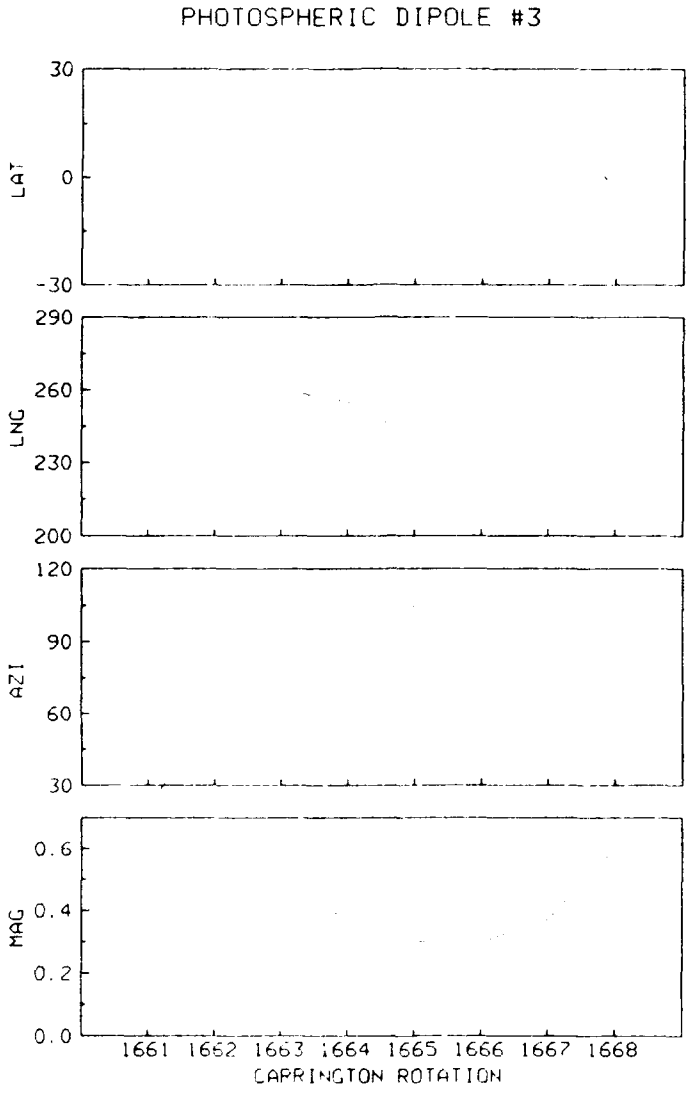
PHOTOSPHERIC DIPOLE #3
LAT
30
0
-30
LNG
290
260
230
200
AZI
120
90
60
30
MAG
0.6
0.4
0.2
0.0
1661 1662 1663 1664 1665 1666 1667 1668
CARRINGTON ROTATION

FIGURE 16

4. CONCLUDING REMARKS

The modern prediction scheme of geomagnetic storms must be based on numerical methods, not on statistical methods. We believe that we have formulated the entire scheme which consists of these computational steps. Our scheme is applicable for a complicated situation in which many flares take place in a relatively short period, say one week. Although much refinement is no doubt needed in the future, we believe that the general scheme is well established by the present project. We have also introduced successfully interplanetary scintillation observations into the scheme to increase the accuracy of the prediction. Most of the refinements require future advance in the field of solar physics, solar wind physics and magnetospheric physics.

One of the critical progresses needed in the prediction is a better understanding of the nature of variations of the polar angle θ of the interplanetary magnetic field. At the present time, it is not known how the variations are caused, although some researchers consider them in terms of 'magnetic clouds' and 'driver gas.'

The present project has also formulated the prediction method of the 27-day recurrent geomagnetic storms. We have shown that the envelope of the 27-day AE index variations can be predicted by predicting variations of the neutral line on the source surface of the sun. The method is simple enough to put into practice.

REFERENCES

Akasofu, S.-I., Energy coupling before the solar wind and the magnetosphere, Space Sci. Rev., 28, 121, 1981.

Akasofu, S.-I. and C. F. Fry, A first generation numerical geomagnetic storm prediction scheme, Planet. Space Sci., 34, 77, 1986.

Akasofu, S.-I., C. Olmsted, T. Saito and T. Oki, Quantitative forecasting of the 27-day recurrent magnetic activity, Planet. Space Sci., 36, 1133, 1988.

Akasofu, S.-I., A note on variations of the IMF Bz and the AE index between 1966 and 1984 in terms of monthly and yearly mean values, Planet. Space Sci., 36, 829, 1988.

Akasofu, S.-I. and Li-Her Lee, A study of the interplanetary disturbances on 1-4 April 1979, Planet. Space Sci., 36, 669, 1988.

Akasofu, S.-I. and Li-Her Lee, Modeling of an interplanetary disturbance event tracked by the interplanetary scintillation method, Planet. Space Sci., 37, 73, 1989.

Akasofu, S.-I. and Li-Her Lee, Modeling of a series of interplanetary disturbance events in September 1978, Planet. Space Sci., 38, 575, 1990.

Akasofu, S.-I., D. Weimer, T. Iijima, B.-H. Ahn and Y. Kamide, Agreements between ground-based and satellite-based observations, Planet. Space Sci., 38, 1533, 1990.

Anderson, K. A., R. P. Lin, D. W. Potter and H. D. Heetderks, An experiment to measure interplanetary and solar electrons, IEEE Trans. Geosa. Elec. GE-16, 153, 1978.

Arnoldy, R. L., Signature in the interplanetary medium for substorms, J. Geophys. Res., 76, 5189, 1971.

Baker, D. N., E. W. Hones, Jr., J. B. Payne and W. C. Feldman, A high time resolution study of interplanetary parameter correlation with AE, J. Geophys. Res., 86, 179, 1981.

Bame, S. J., J. R. Asbridge, W. C. Feldman, J. T. Gosling and R. D. Zwickl, Bi-directional streaming of solar wind electrons >80eV: ISEE evidence for a closed-field structure within the driver gas of an interplanetary shock, Geophys. Res. Lett., 8, 173, 1981.

Borrini, G., J. T. Gosling, S. J. Bame and W. C. Feldman, Helium abundance enhancements in the solar wind, J. Geophys. Res., 87, 7370, 1982a.

Borrini, G., J. T. Gosling, S. J. Bame and W. C. Feldman, An analysis of shock wave disturbances observed at 1 a.u. from 1971 through 1978, J. Geophys. Res., 87, 4365, 1982b.

Burlaga, L. F., L. Klein, N. R. Sheeley, Jr., D. J. Michels, R. A. Howard, M. J. Koomen, R. Schwenn and H. Rosenbauer, A magnetic cloud and a coronal mass ejection, Geophys. Res. Lett., 9, 1317, 1982.

Cane, H. V., R. G. Stone, J. Fainberg, J. L. Steinberg and S. Hoang, Type II solar radio events observed in the interplanetary medium, Solar Phys., 78, 187, 1982.

Chao, J. K. and R. P Lepping, A correlative study of ssc's, interplanetary shocks, and solar activity, J. Geophys. Res., 79, 1799, 1974.

Clauer, C. R., R. L. McPherron, C. Searls and M. G. Kivelson, Solar wind control of auroral zone geomagnetic activity, Geophys. Res., Lett., 8, 915, 1981.

Dryer, M., Some effects of finite electrical conductivity on solar flare-induced interplanetary shock waves, Cosmic Electrodynamics, 11, 348, 1970.

Dryer, M. and R. S. Steinolfson, MHD solution of interplanetary disturbances generated by simulated velocity perturbations, J. Geophys. Res., 81, 5413, 1976.

Dryer, M., S. T. Wu, G. Gislason, S. M. Han, Z. K. Smith, J. F. Wamp, D. GF. Smart and M. A. Shea, Magnetohydrodynamic modeling of interplanetary disturbances between the sun and the earth, Astrophys. Space Sci., V. 105, 187, 1984.

Gosling, J. T., V. Pizzo and S. J. Bame, Anomalously low proton temperatures in the solar wind following interplanetary shock waves: Evidence on magnetic bottles? J. Geophys. Res., 78, 2001, 1973.

Gosling, J. T., E. Hildner, R. M. MacQueen, R. H. Munro, A. I. Poland and C. L. Ross, Mass ejections from the sun: A view from Skylab, J. Geophys. Res., 79, 4581, 1974.

Gosling, J. T., J. R. Asbridge, S. J. Bame, W. C. Feldman and R. D. Zwickl, Observations of large fluxes of He^+ in the solar wind following an interplanetary shock, J. Geophys. Res., 85, 3431, 1980.

Hakamada, K., Three-dimensional structure of the coronal magnetic field and the solar wind speed distribution projected on the photosphere in 1974, J. Geophys. Res., 92, 4339, 1987.

Hildner, E., J. T. Gosling, R. T. Hansen and J. D. Bohlin, The sources of material comprising a mass ejection coronal transient, Solar Phys., 45, 363, 1975.

Hildner, E., J. T. Gosling, R. M. MacQueen, R. H. Munro, A. I. Poland and C. L. Ross, frequency of coronal transients and solar activity, Solar Phys., 48, 127, 1976.

Hirshberg, J., A. Alksne, D. S. Colburn, S. J. Bame and A. J. Hundhausen, Observations of a solar flare induced interplanetary shock and helium-enriched driver gas, J. Geophys. Res., 75, 1, 1970.

Hirshberg, J., S. J. Bame and D. E. Robbins, Solar flares and solar wind helium enrichments: July 1965 - July 1967, Solar Phys., 23, 467, 1972a.

Hirshberg, J., J. R. Asbridge and D. E. Robbins, Velocity and flux dependence of solar wind helium abundance, J. Geophys. Res., 77, 3583, 1972b.

Hoeksema, J. T., J. M. Wilcox and P. H. Scherrer, Structure of the heliospheric current sheet in the early portion of sunspot cycle, 21, J. Geophys. Res., 87 10331, 1982.

Hoeksema, J. T., J. M. Wilcox and D. H. Scherrer, the structure of the heliospheric current sheet: 1978-1982, J. Geophys. Res., 88, 9910, 1983.

Hundhausen, A. and R. A. Gentry, Numerical simulation of flare-generated disturbances in the solar wind, J. Geophys. Res., 74, 2908, 1969a.

Hundhausen, A. and R. A. Gentry, Effects of solar flare duration on a double shock fair at 1 a.u., J. Geophys. Res., 74, 6229, 1969b.

Joselyn, J. A. and J. F. Bryson, Jr., Magalert, August 27, 1978, in Solar and Interplanetary Dynamics, Ed. by M. Dryer and E. Tandberg-Hanssen, p. 413, D. Reidel, Hingham, Mass., 1980.

Joselyn, J. A. and P. S. McIntosh, Disappearing solar filaments: A useful predictor of geomagnetic activity, J. Geophys. Res., 86, 4555, 1981.

Kahler, S. W., N. R. Sheeley, Jr., R. A. Howard, M. J. Koowen, D. J. Michaels, R. E. McGuired, T. T. von Rosenvinge and D. V. Reams, Associations between coronal mass ejections and solar energetic proton events, J. Geophys. Res., 89, 9683, 1984a.

Klein, L. W. and L. F. Burlaga, Interplanetary magnetic clouds at 1 a.u., J. Geophys. Res., 87, 613, 1982.

Liu, Z. X., L.-C. Lee, C. Q. Wei and S.-I. Akasofu, Magnetospheric substorms: an equivalent circuit approach. J. Geophys. Res., 93, 7366, 1988.

Meloni, A., A. Wolfe and L. J. Lanzerotti, On the relationship between interplanetary quantities and the global auroral electrojet index, J. Geophys. Res., 87, 119, 1982.

Meng, C.-I., B. Tsurutani, K. Kawasaki and S.-I. Akasofu, Cross-correlation analysis of the AE index and the interplanetary magnetic field B_z component, J. Geophys. Res., 78, 617, 1973.

Neugebauer, M., Observations constraints on solar wind acceleration mechanisms, Solar Wind Five, p. 135, Ed. by M. Neugebauer, NASA Conf. Pub. 2280, NASA, Washington, D.C., 1983.

Perreault, P. and S.-I. Akasofu, A study of geomagnetic storms, Geophys. J. R. Astronomy Soc., 54, 547, 1978.

Potter, D. W., Acceleration of electron by interplanetary shocks, J. Geophys. Res., 86, 11,111, 1981.

Reiff, P. H., R. W. Shapiro and T. W. Hill, Dependence of polar cap potential drop on interplanetary parameters, JGR 86, 7639, 1981.

Russell, C. T. and R. L. McPherron, The magnetotail and substorms, Space Sci. Rev., 15, 205, 1973.

Saito, T., T. Oki, S.-I. Akasofu and C. Olmsted, The sunspot cycle variations of the neutral line on the source surface, J. Geophys. Res., 94, 5453, 1989.

Saito, T., T. Oki, C. Olmsted and S.-I. Akasofu, A representation of the magnetic neutral line on the solar source surface in terms of the sun's axial dipole at the center and two equatorial dipoles in the photosphere, J. Geophys. Res., 94, 14,993, 1989.

Saito, T., Y. Kozuka, T. Oki and S.-I. Akasofu, On the nature of the photospheric dipoles of the triple dipole model of the solar source surface field, J. Geophys. Res., (submitted), 1990.

Sanahuja, B., V. Domingo, K.-P. Wenzel, J. A. Joselyn and E. Keppler, A large proton event associated with solar filament activity, Solar Phys., 84, 321, 1983.

Schwenn, R., Direct correlations between coronal transients and interplanetary shocks, Space Sci. Rev., 34, 85, 1983.

Sheeley, N. R., Jr., R. A. Howard, M. J. Koomen and D. J. Michels, Associations between coronal mass ejections and soft x-ray events, Ap. J., 272, 349, 1983.

Sheeley, N. R., Jr., R. A. Howard, M. J. Koomen, D. J. Michels, R. Schwenn, K. H. Mulhauser and H. Rosenbauer, Coronal mass ejections and interplanetary shocks, J. Geophys. Res., 90, 163, 1985.

Smart, D. F. and M. A. Shea, A Simplified model for timing the arrival of solar flare-initiated shocks, J. Geophys. Res., 90, 183, 1985.

Smith, E. J., Observations of interplanetary shocks: Recent progress, Space Sci. Rev., 34, 101, 1983.

Tsurutani, B. T. and C.-I. Meng, Interplanetary magnetic field variations and substorm activity, J. Geophys. Res., 77, 2964, 1972.

Wang, S., L.-C. Lee, C. J. Wei and S.-I. Akasofu, A mechanism for the formation of plasmoids and kink waves in the heliospheric current sheet, Solar Phys., 117, 157, 1988.

Wang, Y.-M. and N. R. Sheeley, Jr., Solar wind speed and coronal flux-tube expansion, Astrophys. J., 355, 726, 1990.

Wei, C. J., L.-C. Lee, S. Wang and S.-I. Akasofu, The evolution of magnetic flux ropes associated with flux transfer events and interplanetary magnetic clouds, J. Geophys. Res., (submitted) 1990.

Wilcox, J. A., The daytime F-layer trough and its relation to ionospheric-magnetospheric convection, J. Geophys. Res., 94, 17,169, 1989.

Wilcox, J. M., J. T. Hoeksema and P. H. Scherrer, Origin of the warped heliospheric current sheet, Science, 209, 603, 1980.

Wright, C. S. and L. F. McNamara, The relationships between disappearing solar filaments, coronal mass ejections and geomagnetic activity, Solar Phys., 87, 401, 1983.

Wu, S. T., M. Dryer and S. M. Han, Interplanetary disturbances in the solar wind produced by density, temperature, or velocity pulses at 0.08 AU, Solar Phys., 49, 187, 1976.

Wu, S. T., M. Dryer and S. M. Han, Non-planar MHD model for solar flare-generated disturbances in the heliospheric equatorial plane, Solar Phys., 84, 395, 1983.

Zirker, J. B. (Ed.), Coronal Holes and High Speed Wind Storms, Colorado Associated Univ. Press, 1977.

Zwickl, R. D., J. R. Asbridge, S. J. Bame, W. C. Feldman, J. T. Gosling and E. J. Smith, Plasma properties of driver gas following interplanetary shocks observed by ISEE-3, p. 711, Solar Wind Five, Ed. by M. Neugebauer, NASA Conf. Pub. 2280, NASA, Washington, D.C. 1983.